Repeated slip along a major decoupling horizon between crustal-scale nappesof the Central Western Carpathians documented in the Ochtinà tectonicmélange

N. Novotna, P. Jerabek, Pavel Pitra, O. Lexa, M. Racek

Repeated slip along a major decoupling horizon between crustal-scale nappes of the Central Western Carpathians documented in the Ochtiná tectonic mélange

N. Novotná[1,2], P. Jeřábek[1], P. Pitra[2], O. Lexa[1], M. Racek[1]

1. Institute of Petrology and Structural Geology, Charles University, Albertov 6,128 43 Praha 2, Czech Republic

2. Géosciences Rennes, Université Rennes 1, 35042 Rennes, France

Corresponding author: N. Novotná, Institute of Petrology and Structural Geology, Charles University, Albertov 6,128 43 Praha 2, Czech Republic. (novotna@natur.cuni.cz), phone: +420 22195 1524

Abstract

The Ochtiná Unit is situated in the ENE-WSW-trending contact zone between two crustal-scale nappes, the upper Gemer Unit and the lower Vepor Unit, in the Central Western Carpathians, Slovakia. The Ochtiná Unit consists mainly of Carboniferous phyllitic schists and sandstones enclosing lenses of diverse lithological nature and contrasting metamorphic history. Peak PT conditions obtained by means of phase equilibrium modelling from lenses of amphibolite and chloritoid schist in this unit indicate 500-600 °C and 4-6.5 kbar and 500-520 °C and 9-11 kbar, respectively. These PT conditions contrast not only with the greenschist-facies metamorphism of dominant phyllite but also with each other documenting two distinct metamorphic field gradients related to Variscan and Alpine metamorphic events. Geochemical data reveal an affinity of the amphibolite lenses to similar Variscan rocks in the basement of the upper Gemer Unit and of the

chloritoid schist to similar Alpine rocks in the cover of the lower Vepor Unit. Such heterogeneous lithological and metamorphic record is consistent with a block-in-matrix rock arrangement and the Ochtiná Unit is interpreted as deep seated tectonic mélange. The mélange evolved via repeated slip along the rheologically weak sediments of the Ochtiná Unit during the building and collapse of the Eo-Alpine orogenic wedge of the Central Western Carpathians. Deformation record indicates that the mélange separates two distinct structural domains marked by a decoupled behaviour, i.e. the orogenic suprastructure represented by the Gemer Unit and the infrastructure represented by the Vepor Unit. With this respect, the Ochtiná Unit represents an unusual example of a suprastructure-infrastructure transition zone with its position being controlled by the mechanical weakness of this sedimentary horizon and not by the temperature-dependent rheological transition.

Keywords: Tectonic mélange; phase equilibrium modelling; amphibolite; chloritoid schist; Central Western Carpathians; orogenic wedge

Highlights:

- Heterogeneous lithological record of blocks in matrix is interpreted as a mélange
- Contrasting metamorphic conditions of blocks in the tectonic mélange were revealed
- The mélange separates orogenic Gemer suprastructure and Vepor infrastructure
- The mélange documents repeated slip along mechanically weak horizon

1. Introduction

A mélange is defined as a rock body containing exotic blocks without internal strata continuity.

Mélanges can form in different geological environments. Recently, six main categories of mélanges were distinguished, based on the process and geodynamic context of their formation (Festa et al., 2010 and references therein) and classified into those related to extensional tectonics, passive margin evolution, strike-slip tectonics, subduction zones, collisional tectonics, and intracontinental deformation.

The Ochtiná Unit is located along the boundary between the Gemer and Vepor Units (Central Western Carpathians, Slovakia), in the ENE-WSW-trending so-called Gemer-Vepor Contact Zone. It comprises Carboniferous syn- to late-orogenic sediments, which deposited in a narrow orogenic foredeep basin described as the Nötsch-Veitsch-Szabadbattyán-Ochtiná Zone (Neubauer and Vozárová, 1990). The Ochtiná Unit has its counterpart in the Eastern Alps represented by the so-called Veitsch nappe (Neubauer and Vozárová, 1990). The Ochtiná Unit consists of a complex lithological assemblage with large amount of meter- to hectometer-sized blocks embedded in a dark flysch-like phyllite matrix. Blocks consist of amphibolite, serpentinite, magnesite and Visean to Serpukhovian limestone (Kozur et al., 1976), as well as chloritoid schists and the actinolite-chlorite schists. This complex block-in-matrix assemblage, characterized by the mixing of polymictic blocks of exotic nature with respect to the matrix, closely resemble a tectonic mélange formed at deep structural levels (Festa et al., 2010 and references therein), associated with the Gemer and Vepor nappes stacking. The goal of this study is to test this hypothesis.

In this study we focus on the characterization of a complex lithological assemblage present in the Ochtiná Unit. We provide geochemical data to characterize the sedimentary origin of the

dominant phyllites in this complex. Furthermore, detailed petrological analysis of amphibolites and chloritoid schists from lenticular blocks enclosed in phyllite points out contrasting pressure–temperature (P–T) evolution possibly related to tectonic mixing of mutually incompatible rocks from different tectonic units. The structural record in the Ochtiná Unit identifies this zone as one of the major Eo-Alpine thrust and detachment zones in the Western Carpathians.

2. Geological setting

The Western Carpathians represent the northernmost segment of the European Alpine belt that connects the Eastern Alps to the west and the Eastern Carpathians to the east. The Central Western Carpathians comprise three major crystalline basement units, from the north to the south, the Tatra, Vepor and Gemer Units (e.g. Matějka and Andrusov, 1931; Froitzheim et al., 2008 and references therein, Fig. 1a). These units represent segments of the Variscan crust overlain by Late Palaeozoic–Mesozoic cover, which were amalgamated and tectonically overlain by allochthonous Mesozoic nappes during the Cretaceous Eo-Alpine convergence (Plašienka et al., 1997, Fig. 1).

The Tatra Unit comprises variscan high-grade crystalline basement with its Late Paleozoic to Mesozoic sedimentary cover. It is overlain by a superficial nappe system represented by the structurally lower Krížna nappe and structurally upper Choč nappe, which also overlays the northern part of the Vepor Unit (Fig. 1a). The Krížna and Choč nappes are composed of Mesozoic sedimentary sequences dominated by Triassic carbonate platform sediments (Michalík et al., 1996). It is generally accepted that the Krížna nappe represents a sedimentary infill of the

Zliechov basin originally located between the present day Tatra and Vepor units (Prokešová et al., 2012 and references therein). On the other hand, the location of the basin associated with the Choč nappe has not been resolved (e.g. Tomek, 1993; Plašienka, 2003).

The studied region straddles the Gemer – Vepor Contact Zone (Figs. 1 and 2) and comprises three Alpine units/nappes. The structurally lower Vepor Unit consists of Variscan basement rocks dominated by micaschists (Hladomorná Dolina Complex, Klinec, 1966), intruded by Carboniferous granitoids (Bibikova et al., 1988; Michalko et al., 1998). In the southern and central part of the Vepor Unit, the basement rocks are overlain by the para-autochthonous Permian–Triassic cover comprising meta-arkose, meta-conglomerate and quartzite (Foederata unit, Rozlozsnik, 1935), as well as minor kyanite-chloritoid-bearing schists (Lupták et al., 2003; Vrána, 1964). The structurally intermediate Ochtiná Unit (also called the Ochtiná "nappe"; Kozur and Mock, 1997) represents a few kilometres wide ENE-WSW trending belt located at the border between the Gemer and Vepor Units (Figs. 1b and 2b). The Ochtiná Unit shows a complex lithological assemblage dominated by dark flysch-like phyllites and meta-sandstones, which enclose metric to hectometric lenses of amphibolite, serpentinite, chloritoid schists, magnesite and Visean to Serpukhovian limestone (Abonyi, 1971; Kozur et al., 1976; Němejc, 1946). The carbonates are usually interpreted as part of the Ochtiná sedimentary sequence while the other rocks are commonly seen as exotic (e.g. Vozárová, 1990). Although this complex was earlier interpreted as the Lower Carboniferous cover of the Gemer Unit (Němejc, 1946; Planderová and Vozárová, 1978), more recently a separate evolution of the Ochtiná Unit was proposed based on the study of fluid inclusions and possible correlation of lithostragraphic horizons (Kozur and Mock, 1997; Németh et al., 2006). Further to the east, the Gemer-Vepor

Contact Zone is marked by a similar lithological complex – the Črmel nappe (e.g. Vozárová, 1996; Grecula et al., 2009). The structurally upper Gemer Unit is dominated by a basement comprising three groups with distinct lithology and metamorphic grade (Faryad, 1991a; Grecula, 1982). The structurally uppermost Gelnica group in the south comprises volcano-sedimentary rocks intruded by Permian granitoids (Grecula, 1982; Poller et al., 2002) the structurally lower Rakovec group is dominated by metavolcanites (Hovorka and Ivan, 1985), and the lowermost Klátov group in the north consists of paragneiss and amphibolite (Faryad, 1990; Hovorka et al., 1997). The Gelnica and Rakovec groups are uncomfortably overlain by Upper Carboniferous shales and Permian meta-conglomerates (Šucha and Eberl, 1992). The Gemer Unit is tectonically overlain by the Meliata subduction-accretionary complex of Jurassic age (Faryad and Henjes-Kunst, 1997; Mock et al., 1998) and by the uppermost Triassic Turňa and Silica nappe systems (Fig. 1b).

The Variscan metamorphic fabrics of greenschist- to amphibolite-facies grade are dominant in the Gemer Unit (e.g. Faryad, 1995). Maximum P–T conditions are documented in the Klátov complex (550-700 °C at 7-10 kbar, Faryad, 1995), intermediate P–T in the Rakovec complex (440-480 °C at 7-10 kbar, Faryad, 1999) and low P–T in the Gelnica complex (up to 350-450 °C at 3-5 kbar, (Faryad, 1994). The Variscan metamorphism in the southern Vepor basement reached 570-670 °C at 6-8.5 kbar (Jeřábek et al., 2008).

The Cretaceous tectono-metamorphic overprint was higher grade and more intense in the Vepor Unit than in the Gemer Unit. In the Gemer Unit, the Alpine metamorphic overprint reached generally lower greenschist-facies conditions (330-350 °C at 4.5-6 kbar in the Permian granitoids, Faryad and Dianiška, 1999) and 200-250 °C in the cover (Šucha and Eberl, 1992). In

the Vepor basement, the Alpine metamorphic conditions range in a variety of P–T conditions depending on the structural position of the studied samples (430-620 °C at 5-11 kbar; Janák et al., 2001; Jeřábek et al., 2012, 2008; Plašienka et al., 1999). In the Gemer-Vepor Contact Zone (Fig. 2), the Alpine metamorphism reached 520-550 °C at 8-9 kbar in the basement schists (Jeřábek et al., 2008). The P–T conditions in the Foederata cover overlying the central portion of the Vepor basement are 350-400 °C at 4-4.5 kbar (Lupták et al., 2003), whereas in the Gemer-Vepor Contact Zone the Permian cover recorded 530-560 °C at 4.5-8 kbar (Lupták et al., 2000), similar to the underlying Vepor basement schists.

3. Structural record in the Gemer-Vepor Contact Zone

Four major deformation fabrics were distinguished in the Gemer-Vepor Contact Zone: (i) heterogeneously preserved Variscan metamorphic fabric S_V, (ii) main Alpine deformational fabric S_{A1}, and (iii) and (iv) heterogeneously developed Alpine fabrics S_{A2} and S_{A3} (Fig. 2). The three Alpine fabrics document the polyphase Cretaceous evolution of the studied area. In the studied area, the Gemer-Vepor Contact Zone is marked by nearly 45° change in trend of the dominant lithological belts (Fig. 2b), from ENE-WSW in the NE to NNE-SSW in the SW. For this reason, individual deformation structures in figure 2a are shown separately for the domains marked by ENE-WSW trend (solid symbols), and NNE-SSW trend (open symbols), respectively.

In the Vepor basement schists, the Variscan metamorphic foliation S_V comprises garnet-biotite-plagioclase-muscovite-quartz (Fig. 3a) and it is mainly preserved in the north, close to the contact with the leucogranite (Fig. 2), which intrudes the schists and forms numerous dykes

crosscutting the S_V fabric. The S_V fabric in this region is generally SE-dipping at various angles due to the subsequent Alpine deformation overprint (Fig. 2a, c). Both the schists and the leucogranite are overprinted by the first Alpine metamorphic fabric S_{A1} comprising grossular-rich garnet, biotite, albite, epidote, white mica and quartz (Fig. 3a). The heterogeneous development of the S_{A1} fabric in the leucogranite and the neighbouring schists contrasts with its pervasive development and the associated complete obliteration of the Variscan foliation S_V by the S_{A1} cleavage towards the SE (Fig. 2c). Further to the SE, in the vicinity of the Permian Vepor cover, the S_{A1} fabric is isoclinally folded and overprinted by a lower grade muscovite- and chlorite-bearing second Alpine cleavage S_{A2} (Fig. 2c and 3b). Here the S_{A1} and S_{A2} cleavages are subparallel and generally SE-dipping (Fig. 2a, c). Both fabrics bear a mineral and stretching lineation defined by the shape of mica and quartz aggregates. The Veporic Permian cover shows two deformation fabrics S_{A1} and S_{A2} associated with distinct metamorphic grade marked by higher grade chloritoid-kyanite and lower grade chlorite-muscovite assemblages in the schist as well as distinct quartz deformation microstructures in the meta-arkose (Bukovská et al., 2013). The superposition of the two fabrics leads to the common development of S-C-type geometries (Fig. 3c). Towards the southern contact with the hanging wall Ochtiná Unit, the S_{A1} and S_{A2} cleavages become locally overprinted by kink bands and open folds F_3 with generally ENE-WSW trending axial planes S_{A3} (Fig. 2a). The phyllites of the Ochtiná Unit show a complex polyphase deformation with relics of the higher-grade fabric S_{A1} being mostly obliterated by the lower-grade muscovite-chlorite bearing S_{A2} cleavage (Figs. 2c, 3d, e), and subsequent F_3 folding associated with local development of very low-grade cleavage S_{A3} (Fig. 3f). F_3 folds have subhorizontal axes and their axial planes, parallel to the S_{A3} cleavage, are steep and generally

ENE-WSW trending (Fig. 2b, 2c and 3f). In all the above-described lithologies, the S_{A1} and S_{A2} fabrics are subparallel and their poles are distributed along broad girdles related to the development of the F_3 folds (Fig. 2a). In places where the main lithological belts are WSW-ENE-trending (Figs. 1b and 2b), the girdles are oriented NNW-SSE, whereas where the belts are NNE-SSW-trending, the girdles are oriented WNW-ESE (cf. solid and open symbols in Fig. 2a). Accordingly such change in orientation also applies to the intersections of S_{A1} and S_{A2} showing parallel orientation to the trend of the belts. In contrast, lineations L_{A1} and L_{A2} do not change their orientation with changing trend of the foliations. L_{A1} is oriented WSW-ENE to SW-NE whereas L_{A2} is roughly E-W trending (Fig. 2a). This suggests that the changes in trends of the lithological belts and S_{A1} and S_{A2} fabrics do not result from subsequent folding but more likely reflect the shape of the underlying Vepor basement. The Gemer basement in the studied area shows relics of Variscan metamorphic fabric S_V (Fig. 2a), which are nearly completely obliterated by the lower grade muscovite- and chlorite-bearing cleavage S_{A1}. This S_{A1} cleavage generally dips to the south at variable angles ranging from steep to shallow. S_{A1} cleavage in the Permian conglomerates of the Gemer cover is steep and E-W trending, and overprints subhorizontal bedding. In contrast to the Vepor Unit, S_{A2} cleavage was not identified in the studied portion of the Gemer Unit. Orientations of both S_V and S_{A1} fabrics in the Gemer Unit were subsequently modified by larger scale folds F3 with steep, generally E-W trending axial planes and subhorizontal axes (Fig. 2a). Also, several localized transpressional zones associated with left-lateral movements develop within the Vepor and Gemer basements.

The blocks of heteregeneous lithologies found in the Ochtiná Unit have in general elongated, lenticular shape with long axes parallel to main foliations S_{A1} and S_{A2} as well as to locally

developed S_{A3}. Although the size of these blocks varies, both the small meter-sized blocks as well as large (up to several hundred meters) blocks are wrapped by the phyllite matrix. Due to the limited number of outcrops, the extent of the larger blocks is only documented by geological mapping. Because it is not clear from the field observations which of the fabrics is responsible for incorporation of the blocks into phyllite matrix a detailed petrographic-petrological study had been carried out.

4. Lithological characterization of the Ochtiná Unit

In order to understand the tectonic evolution of the Ochtiná Unit, the petrologically most informative lithologies were sampled and analysed to check the supposed mélange character of the unit. These include the dominant phyllites, as well as chloritoid schists, amphibolites, serpentinites and actinolite schists sampled from the lenticular blocks (Fig. 1). Because very little is known about the primary depositional environment of the phyllites of the Ochtiná Unit, five samples were collected for geochemical characterization of these rocks (Fig. 1b).

4.1 Analytical techniques

Whole rock chemical compositions were obtained from the ACME Labs, Vancouver, Canada. Samples were finely ground in an agate tray and the whole rock major and minor elements compositions were obtained by ICP-ES following a lithium borate fusion and dilute acid digestion of a 0.2 g pulp. Trace element contents were obtained by ICP-MS. The analyses are

presented in Tables 1 and 2. Detection limits for major elements are 0.01 %, for the trace elements the detection limit varies from 0.01 ppm (Hg) to 1 ppm (Ba, Be, Sn).

Mineral compositions were determined using the electron microprobe Cameca SX100 in wavelength-dispersive mode at the Joint Laboratory of Electron Microscopy and Microanalysis, of the Masaryk University, Brno, and the Czech Geological survey and scanning electron microscope TESCAN Vega with energy-dispersive spectrometer X-MAX 50 (silicon drift detector, SDD) from Oxford Instruments controlled by the INCA software at the Institute of Petrology and Structural Geology, Charles University in Prague. On both instruments, the analyses were obtained with an accelerating potential of 15 kV and a beam current of 1 nA for the TESCAN Vega and a beam current of 20 nA for the Cameca SX100. The precision control was held by repeated measurements of known phases, mainly standards.

4.2 Phyllites

The phyllites are the dominant lithology of the Ochtiná Unit. They have a well developed slaty cleavage S_{A1} with local overprint by cleavage S_{A2} (Fig. 3d). The slaty cleavage S_{A1} is marked by the preferred orientation of fine-grained white mica and chlorite and locally graphite. The foliation is anastomosing around stronger domains of quartz or larger crystals of mica. Calcite, tourmaline, plagioclase, hematite, ilmenite, rutile, zircon and monazite are locally present. The size of the crystals ranges from 0.1 mm to 0.5 mm.

Based on the whole rock analyses, the studied phyllites show a relatively wide compositional

range (Tab. 1). The SiO_2/Al_2O_3 index, used to characterize the sedimentary maturation, ranges from 2.7 to 5.2 – close to values characteristic for igneous source rocks (Roser et al., 1996). On the other hand, the rather diverse character of the studied phyllites may indicate both basic (SiO_2/Al_2O_3 = 2.7-3.6, samples NN123, NN142 and TU5) and acidic source rocks (SiO_2/Al_2O_3 ~ 5.2, samples NN135 and R40), and/or sedimentary maturation in the latter case.

Compared to the Upper Continental Crust standard (UCC after Rudnick and Gao, 2003; Tab. 1), the phyllites are depleted in Na_2O and CaO – except for sample NN123 (Tab. 1) characterized by high calcite and apatite contents. The transition elements, large ion litophile (LIL), high field strength (HFS) and rare earth elements (REE) show values comparable to the UCC. To discuss the tectonic setting and the source rocks for the sedimentary protolith of the phyllites, the discrimination diagrams of Floyd and Leveridge (1987) and Bhatia and Crook (1986) were used. In the diagram La/Th vs. Hf , the analyzed samples show proximity to the acidic arc source field (Fig. 4a). In the Ti/Zr vs. La/Sc and La-Th-Sc-Zr/10 diagrams (Fig. 4b and c), most phyllite samples exhibit an affinity to continental arc source. An exception is sample NN123, which differs significantly from the rest of studied samples (see Table 1) and indicates an island arc affinity (Fig. 4b and 4c).

4.3 Chloritoid schists

Chloritoid schists are fine-grained quartz- and white mica-dominated rocks (Fig. 5a-c). They display a compositional layering with layers rich in chloritoid and white mica and layers rich in chlorite and quartz. Layering is parallel to a foliation defined by the preferred orientation of

muscovite (Si = 3.04-3.07 a.p.f.u, X_{Na}= $Na_2O/(Na_2O+K_2O)$ = 0.13-0.15, Fig. 5a). Deformed porphyroclasts of muscovite (up to 0.5 mm) wrapped by the foliation are locally present. Paragonite (X_{Na} = 0.74-0.85, X_{Ca} = 0-0.2) occurs locally in close association with chloritoid and it commonly intergrows with muscovite (Fig. 5c). Recrystallized quartz aggregates (up to 1 mm) stretched parallel to and wrapped by the foliation are common. Chloritoid (X_{Mg} = $Mg/(Fe^{2+}+Mg)$ = 0.14-0.15) forms euhedral prismatic unzoned porphyroblasts (up to 0.3 mm, Fig. 5a and c), commonly associated into radial aggregates up to 1 mm in size (Fig. 5a). Aggregates and individual crystals are typically wrapped by the foliation, but crystals parallel to the foliation are also common. Ilmenite, rutile and quartz form inclusions in chloritoid (Fig. 5c). Chlorite (X_{Mg} = 0.36-0.40) forms flakes (≈0.5 mm) parallel to the foliation. Chlorite is very rare in the chloritoid-rich layers and vice versa. However, around the interface of both types of layers, chloritoid and chlorite coexist in an apparent textural equilibrium. Additionally, the foliation contains subhedral prisms of tourmaline, ilmenite, rutile and locally hematite. Based on the microstructural relations the inferred synfolial equilibrium assemblage comprises chloritoid, chlorite, muscovite, paragonite, rutile, ilmenite, hematite and quartz (for representative mineral analyses see Table 2).

4.4 Amphibolites

Amphibolites are homogeneous fine-grained rocks generally lacking preferred orientation and only locally displaying a faint cleavage parallel to discrete micro shear zones (Fig. 5d-f). They contain porphyroblasts of calcic clinoamphibole (up to 1 mm) and titanite (up to 0.5 mm) in a fine grained matrix, which is composed of epidote, plagioclase, titanite and small amounts of

chlorite, clinoamphibole and quartz (Fig. 5d-f, Tab. 2). Amphibole porphyroblasts (Fig. 5f) contain inclusions of titanite and locally also epidote and have a core of actinolite (Si = 7.5-7.8 p.f.u., $X_{Na} = Na_{M4}/(Na_{M4}+Ca)$ = 0.002-0.022, X_{Mg} = 0.61-0.67, recalculated Fe^{3+} = 0.02-0.08, $XAl_{M2} = (Si+Al-8)/2$ = 0.08-0.14), rimmed by hornblende s.l. (Si = 6.3-6.9 p.f.u., X_{Na} = 0.005-0.027, X_{Mg} = 0.45-0.53, XAl_{M2} = 0.37-0.51, Fig. 6). However, in some places actinolite and hornblende are intergrown, without clear core-rim relation (Fig. 5d). Titanite porphyroblasts are locally partly recrystallized to smaller titanite crystals. Epidote forms randomly oriented subhedral prims (0.05-0.5 mm) in the matrix (Figs. 5d and 5f) and commonly displays oscillatory zoning ($X_{Fe3+} = Fe^{3+}/(Fe^{3+}+Al–2)$ = 0.50-0.70). Matrix plagioclase is albite (up to 5 % anorthite) with locally preserved relict cores of oligoclase (10-15 % of anorthite, Fig. 5e). Chlorite (X_{Mg} = 0.50-0.55) is relatively rare in the matrix, but oriented crystals are commonly present in the micro shear zones cross-cutting the sample (Fig. 5d).

Based on the microstructural relations, we infer that the matrix assemblage albite-epidote±actinolite±chlorite overprints an earlier assemblage that comprised oligoclase, hornblende, titanite ± epidote, ± quartz. It is not clear whether actinolite cores of large porhyroblasts were part of this early equilibrium assemblage. While the intergrowths of actinolite with hornblende are in favour of this interpretation, actinolite cores surrounded by hornblende may point to actinolite being the precursor of hornblende along a prograde P–T evolution. The growth of chlorite in the shear zones is interpreted as a late local feature, possibly related to fluid circulation and could be in association with the matrix assemblage.

From the whole rock chemical data, the studied amphibolites enclosed within phyllites of the

Ochtiná Unit show a restricted compositional range (Table 1). Based on the immobile trace elements, the amphibolites correspond to subalkaline basaltic rocks in the Zr-Ti vs. SiO_2 discrimination diagram (Fig. 7a, after Winchester and Floyd, 1977) and indicates transition from N-MORB (mid-ocean ridge basalt) to E-MORB (enriched mid-ocean ridge basalt) in the Th-Hf/3-Ta discrimination diagram (Fig. 7b, after Wood, 1980). In the Zr/Y vs. Zr diagram for basic rocks (Fig. 7c, after Pearce and Norry, 1979), the studied samples also correspond to mid-ocean ridge basalts. In all the diagrams in figure 7a, b, c, the Ochtiná amphibolite is compared with the previously published geochemical data from amphibolites of the Gemer basement (Bajaník, 1976; Ivan, 2008), which show similar affinity to the mid-ocean ridge basalts field and indicate a possible correlation between these amphibolites.

4.5 Serpentinites and actinolite-chlorite schists

The serpentinites are dominated by fine grained serpentine and magnetite. Serpentine flakes (<0.1 mm) are randomly oriented and neither the core-and-rim mesh microstructures, nor bastites are observed. Very fine-grained magnetite is concentrated in thin layers that form an anastomosing network and separate lenses (in general 0.2-0.5 mm long) of nearly pure serpentine. Talc and coarser-grained magnetite (up to 0.5 mm) together with subordinate chlorite fill fractures that crosscut the rock (Fig. 8a). The serpentine lenses probably represent pseudomorphed crystals of olivine. These rocks are interpreted as former peridotites, although no relics of the original minerals or microstructures were found.

An actinolite-chlorite schist crops out in the vicinity of one of the serpentinite bodies. The schist contains 2-10 mm large domains of recrystallised polycrystalline quartz (0.1-0.3 mm) and

domains of oriented, Mg-rich chlorite with numerous tiny grains of titanite, commonly aligned in thin bands. These domains are surrounded by a quartz-chlorite matrix that shows a well developed foliation. The matrix contains thin prismatic crystals of actinolite (up to 1.5 mm long) (Fig. 8b), which are in some cases oriented parallel to the foliation, although, in other occurrences they are wrapped by the foliation and show variable orientations. This peculiar schist may be interpreted as a volcano-sedimentary rock containing quartz pebbles in a matrix of rather mafic composition.

5. P-T estimates

One sample of a chloritoid schist (NN155) and one of an amphibolite (NN25) from two lenses in the Ochtiná Unit were selected for a petrological study based on their suitable mineral assemblage. To obtain P-T estimates from the two samples, P–T pseudosections and compositional isopleths were calculated using the thermodynamic modelling software Perple_X version 6.6.8 (Connolly, 2005) and THERMOCALC version 3.33 (Powell and Holland, 1988). The use of THERMOCALC was preferred because it is more reliable in handling the most up-to-date complex solid solutions, like those for amphiboles. However, it appeared impossible to complete the P–T pseudosection for the chloritoid schist with THERMOCALC because of software problems during calculation of equilibria involving muscovite-paragonite and ilmenite-haematite solvi. Thus Perple_X was used instead for this rock. Nevertheless, the results of the two techniques can be compared, since it has been demonstrated that Perple_X and THERMOCALC yielded identical results when the same thermodynamic dataset was used

(Hoschek, 2013, 2004).

5.1 Chloritoid schist

The P-T pseudosection for chloritoid schist sample NN155 was constructed by using Perple_X (Connolly, 2005) v. 6.6.8 and the internally consistent thermodynamic dataset hp04 (Holland and Powell, 1998) in the model system $MnO-Na_2O-K_2O-FeO-MgO-Al_2O_3-SiO_2-H_2O-TiO_2-Fe_2O_3$ (MnNKFMASHTO). The whole rock composition used to calculate the P-T section is presented in figure 9 and table 1. All CaO (0.04 wt.%) is combined with P_2O_5 to form apatite and therefore CaO component was excluded from the calculation. The amount of O_2 was recalculated from the whole rock composition with respect to the estimated ratio of Fe^{3+}/Fe^{total} 0.05. The mixing models for chloritoid (Holland and Powell, 1998), chlorite (Holland and Powell, 1998), biotite (White et al., 2007), white mica (Auzanneau et al., 2010; Coggon et al., 2002), garnet (White et al., 2000), ilmenite (White et al., 2000) and staurolite (Holland and Powell, 1998) were used. In the resulting P-T pseudosection (Fig. 9), the observed equilibrium assemblage chloritoid, chlorite, muscovite, paragonite, ilmenite, rutile, hematite and quartz corresponds to a narrow stability field ranging between 480-520°C and 7.5-12 kbar. This stability field is limited by the disappearance of rutile towards higher temperatures and by the disappearance of paragonite towards lower pressures and higher temperatures. The modelled compositional isopleths for chloritoid and muscovite were used to further constrain the equilibration P–T conditions (Fig. 9). X_{Mg} in the analysed chloritoid grains ranges 0.14–0.15 yielding a temperature interval of 500-520°C. The Si content in the analysed muscovite ranges 3.04–3.07 a.p.f.u. which corresponds to

9-11 kbar in the calculated P–T pseudosection (Fig. 9).

5.2 Amphibolites

The P–T pseudosection for amphibolite sample NN25 was calculated using THERMOCALC 3.33 (Powell and Holland, 1988) and the internally-consistent thermodynamic dataset 5.5 (Holland and Powell, 2003 upgrade, 1998) in the model system Na_2O-CaO-FeO-MgO-Al_2O_3-SiO_2-H_2O-TiO_2- Fe_2O_3 (NCFMASHTO) for the analysed whole-rock composition (Fig. 10, Table 1). The amount of Fe_2O_3 was analysed by wet chemical titration. Because activity-composition relations for Mn-bearing solid solutions, in particular amphiboles, are poorly constrained and the studied sample has a low MnO content (0.22 wt. %), MnO was not included in the chemical model system. The whole rock composition used to calculate the P-T section is presented in figure 10 and Table 1. K_2O was excluded from the calculation because (i) potassium-bearing micas and K-feldspar are absent in the studied sample, (ii) the existing mixing model for amphibole does not incorporate K_2O and (iii) the amount of K_2O in the studied sample is low (0.1 wt.%; Tab. 2). The mixing models of clinoamphibole (Diener and Powell, 2012), clinopyroxene (Diener and Powell, 2012), chlorite (Holland and Powell, 1998), garnet (White et al., 2007), epidote (Holland and Powell, 1998), plagioclase (Holland and Powell, 2003), ilmenite and hematite (White et al., 2000) were used in the calculation.

In the resulting pseudosection (Fig. 10), the early equilibrium assemblage of hornblende, plagioclase, titanite, ± epidote and quartz corresponds to the stability field spanning between 500-600 °C and 4-7 kbar. For a more precise determination of the peak P-T conditions, the

compositional isopleths of X_{Ca} (= Ca/(Ca+Na)) in plagioclase and the proportion of octahedral Al in hornblende (XAl_{M2}) were calculated. In the pseudosection, both sets of isopleths have an intermediate positive slope. Towards high temperature and low pressure XAl_{M2} in amphibole decreases, whereas X_{Ca} in plagioclase increases. The XAl_{M2} value in the analysed hornblende ranges 0.45-0.50 p.f.u. (Tab. 2) indicating the upper pressure limit of 6.5 kbar (Fig. 10). The analysed plagioclase, inferred to be in equilibrium with hornblende, contains up to 15 % of anorthite component. However, the minimum modelled X_{Ca} value in plagioclase is of ca. 0.20 (Fig. 10) and the analysed values are not modelled in the pseudosection. This could be related to uncertainties on the actual Fe_2O_3/FeO ratio, which is easily affected by late alteration and has influence on the position of the compositional isopleths (e.g. López-Carmona et al., 2013). A P-X_{Fe2O3} pseudosection has been constructed in order to check this influence (Fig. 11). However, even at very low values of Fe_2O_3 the proportion of anorthite in plagioclase does not reach values significantly lower than 0.2. Consequently, we infer that the plagioclase composition must reflect later local partial reequilibration (cf. below). Based on the pseudosection, the peak P-T conditions of the studied amphibolite sample correspond to 500-600 °C at 4-6.5 kbar. The later matrix mineral assemblage of actinolite, epidote, albite and chlorite re-equilibrated in the broad field spanning from the beginning of the section at 400-470 °C and 3-8 kbar (Fig. 10).

6. Discussion

The Ochtiná Unit marks the tectonic contact between the Gemer and Vepor Units in the Central Western Carpathians. It comprises flysch-like phyllites and meta-sandstones that contain diverse

exotic lenticular blocks up to hundreds of meters in size. In earlier concepts, these rocks were considered part of the upper plate Gemer Unit and their sedimentary cover relationship to the Gemer basement has been favoured. The lenticular blocks of amphibolite and serpentinite were associated with imbrications of the Gemer basement (Vozárová, 1990). However, the studied blocks revealed a different metamorphic history and correspond to contrasting transient geothermal gradients (Fig. 12). The equilibration conditions of the amphibolite lens are of 4-6.5 kbar at 500-600 °C, later re-equilibrated at 3-8 kbar and 400-470 °C, whereas the chloritoid schist equilibrated at 9-11 kbar and ~500 °C. Consequently, our results show that the occurrence of exotic strong blocks enclosed within the weak phyllite matrix of the Ochtiná Unit can be regarded as a mappable block-in-matrix rock unit (i.e., mélange sensu Silver and Beutner, 1980; Raymond, 1984; Festa et al., 2012).

6.1. The tectonic significance of the Ochtiná Unit

The Ochtiná Unit and the similar lithological complex of the Črmel nappe further east delineate a major boundary between the crustal scale Vepor and Gemer units. Since Andrusov (1936) this boundary has been recognized as a major thrust of the Gemer Unit over the Vepor Unit. In the studied area, this event is associated with the development of S_{A1} deformation fabrics, which are relatively steep and E-W trending in the Gemer Unit and subhorizontal with an E-W stretching component in the Vepor Unit (Fig. 13a). This process is associated with prograde metamorphism during crustal thickening and burial of the Vepor Unit (Jeřábek et al., 2008; Jeřábek et al., 2012). The development of the S_{A2} fabric is mainly documented in the vicinity of the contact between

the Gemer and Vepor units, but did not affect the hanging wall Gemer Unit. It is interpreted that the Ochtiná Unit localized the detachment responsible for the unroofing of the Vepor basement (Fig. 13b; Plašienka et al., 1999; Janák et al., 2001; Bukovská et al., 2013). Finally, the F3 folding and the heterogeneous development of the S_{A3} fabric can be associated with the localization in the southern part of the Ochtiná Unit of sinistral transpressive movements along the Trans Gemer Shear Zone (Fig. 13c; Lexa et al., 2003).

6.2. Origin of the lithological assemblage in the Ochtiná Unit mélange

Based on the geological, metamorphic and geochemical evidence, the complex lithological assemblage of the blocks in the phyllite matrix of the Ochtiná Unit is associated with three different source regions. 1) The limestone, dolomite and magnesite blocks are interpreted to represent a dismembered carbonate horizon of Lower Carboniferous age within the Ochtiná sedimentary sequence (Abonyi and Abonyiová, 1981). In contrast, 2) the amphibolite and serpentinite blocks show affinity to the Gemer basement while 3) the chloritoid schists are most likely derived from the Vepor cover.

1) Supportive evidence for this interpretation comes from an identical lithological assemblage of flysch sediments and carbonates reported from the Carboniferous Veitsch nappe (Ratschbacher, 1986), which is considered as a counterpart of the Ochtiná Unit in the Graywacke zone of the Eastern Alps (e.g. Neubauer and Vozárová, 1990) and which lacks the complex lithological assemblage recorded in the Ochtiná Unit. The limestones in both nappes locally experienced metasomatic replacement of calcite by dolomite and magnesite that has been associated with

Permian rifting (Prochaska, 2000) or Cretaceous collision (Hurai et al., 2011).

2) Amphibolites are frequent in the Gemer basement mainly in the Rakovec and Klátov complexes and occur in a close proximity to the Gemer-Vepor contact zone (Fig. 1b). Serpentinised peridotites also occur in the Gemer basement (Hovorka and Zlocha, 1974) although little is known about their origin. Estimates of the peak PT conditions of the studied amphibolite in the Ochtiná Unit range between 500-600 °C and 4-6.5 kbar and show very good correlation with the previously published PT data from the Gemer amphibolites (Fig. 12, Faryad, 1995, 1991a). The formation of the Gemer amphibolites is associated with the Variscan tectono-metamorphic event (Faryad, 1990), thus the age of the peak metamorphism in the Ochtiná amphibolite is most likely also Variscan as previously proposed by Vozárová (1990). The correlation of the Ochtiná and Gemer amphibolites is further supported by comparing the geochemical data from the Ochtiná amphibolite (Table 1, Fig. 7) with the previously published data from the Rakovec complex (Bajaník, 1976; Ivan, 2008). Both data sets show relatively good match indicating a mid-ocean ridge to within plate basalts affinity of the analysed amphibolites (Fig. 7). The Ochtiná amphibolite and serpentinite are thus interpreted to represent parts of the upper plate Gemer basement that were incorporated into the Ochtiná phyllites during the Early Cretaceous thrusting of the Gemer Unit over the Vepor Unit (see discussion below).

3) Southern portions of the Vepor Foederata cover, located in direct structural footwall of the overlying Ochtiná Unit, contain chloritoid-kyanite schists (Lupták et al., 2000; Vrána, 1964). These schists probably represent an aluminium-rich sedimentary horizon in the Permian sequence that was subjected to Cretaceous metamorphism. The metamorphic conditions of these

schists range 530-560 °C and 4.5-8 kbar (Lupták et al., 2000) and their Cretaceous (~97 Ma) metamorphic age has been recently constrained by U-Pb dating of monazite (Bukovská et al., 2013). Chloritoid-schists enclosed within the Ochtiná phyllite typically occur close to the boundary with the Vepor Unit (Fig. 1). These rocks show identical microstructural relationships as those described in chloritoid schists of the Vepor cover (Bukovská et al., 2013; Lupták et al., 2000) and are characterized by similar PT conditions of ~ 500°C and 9-11 kbar (Fig. 12). Based on these similarities, the chloritoid schists of the Ochtiná Unit are interpreted as parts of the Vepor cover that were incorporated into the Ochtiná phyllites during the unroofing of the Vepor Unit (see discussion below).

6.3. The mechanism of incorporation of exotic blocks into the Ochtiná Unit mélange

Mélanges related to collisional tectonic settings are capable of incorporating material from both upper and lower plates during a single kinematic event (Festa et al., 2010; Huang et al., 2008; Chang et al., 2001). Careful characterization of the tectono-metamorphic record of the Ochtiná mélange, however, does not allow for a simple kinematic model. Instead, the incorporation of the Gemer and Vepor derived rocks is explained by repeated reactivation along the rheologically weak sediments of the Ochtiná sequence transformed into a major décollement horizon between the two crustal-scale units. Because field observations don't allow to establish a clear structural relationship between the blocks and the surrounding phyllites, this interpretation is based purely on comparison of metamorphic record in the matrix phyllites and incorporated blocks.

The metamorphic overprint associated with the Cretaceous nappe stacking and northward

overthrusting of the Gemer Unit over the Vepor Unit and the development of S_{A1} is of relatively low grade in the Gemer basement (350 °C, 5-6 kbar; Fig. 12; Faryad and Dianiška, 1999) and the underlying Ochtiná Unit. S_{A1}-related micro shear zones in the Gemer-derived blocks of Variscan amphibolites yield 3-8 kbar and 400-470 °C. It is thus likely that it is during the northward overthrusting of the Gemer Unit when the amphibolite blocks have been sheared off from the bottom Gemer basement and incorporated into the Ochtiná phyllites (Fig. 13a).

On the other hand, the PT conditions related to the S_{A1} fabric in the direct footwall of the Ochtiná Unit in the studied area reached up to 9 kbar at 550 °C for the southern Veporic cover and the underlying basement schists (Jeřábek et al., 2008; Lupták et al., 2000). These PT conditions document a metamorphic gap across the boundary between the lower grade Ochtiná Unit in the hanging wall and the higher grade Vepor metasediments in the footwall. Such a metamorphic gap is consistent with the existence of a décollement shear zone associated with the exhumation and unroofing of the Vepor Unit. In the studied area, this décollement is associated with the development of lower grade subhorizontal cleavage S_{A2}, which mainly affected the Vepor cover and Ochtiná phyllite but has not been identified in the hanging wall Gemer Unit (Fig. 13b). Moreover, the blocks of chloritoid schists within the Ochtiná phyllite occur exclusively in the vicinity of the contact with the Vepor Unit and record similar PT conditions as the nearby Vepor cover metasediments. It is thus likely that the top parts of the Vepor Unit have been sheared off and incorporated into the hanging wall Ochtiná phyllites during exhumation of the Vepor Unit (Fig. 13b).

The last Upper Cretaceous deformation phase documented in the studied area corresponds to the

left-lateral transpressional movements between the Gemer and Vepor Units, which are recorded by the development of steep cleavages and shear zones S_{A3} mainly in the Ochtiná phyllites (Lexa et al., 2003). These horizontal movements are again accommodated by the Ochtiná Unit along the southern edge of the Vepor Unit (Fig. 13c). The strike slip derived tectonic mélange (Festa et al., 2010; Dela Pierre et al., 2007) represents an alternative scenario for incorporation of both Gemer and Vepor rocks into the Ochtiná Unit. However, no significant transpressional movements were documented in the Črmel nappe (Lexa et al., 2003) that contains a similar block-in-matrix lithological assemblage and delineates the contact between the Gemer and Vepor units further to the east (Vozárová, 1996).

6.4. The effect of weak décollement horizon on the style of collision between major crustal nappes

The rheological characteristics of the sediments of the Ochtiná Unit dominated by phyllites represent an ideal décollement horizon to promote major relative movements between the neighbouring Gemer and Vepor Units. The repeated reactivation of this horizon may explain the mechanically uncoupled behaviour during deformation documented by the contrasting structural record in the Gemer suprastructure and the Vepor infrastructure (Jeřábek et al., 2012; Lexa et al., 2003). 1) The overthrusting is associated with steep E-W trending cleavages in the Gemer suprastructure and subhorizontal fabrics with characteristic E-W orogen-parallel stretching in the Vepor infrastructure. 2) The unroofing of the Vepor Unit is associated with the development of detachment fabric in the Vepor infrastructure but the suprastructure has not been affected by this

deformation. 3) Several localized transpressional zones associated with left-lateral movements develop within the Vepor and Gemer basements suggesting coupled behaviour of the two units and no major role of the Ochtiná nappe in this late Cretaceous process.

It is concluded that the Ochtiná décollement zone served repeatedly as a high-strain shear zone promoting decoupled behaviour between the orogenic suprastructure and infrastructure in the Eo-Alpine West Carpathians orogenic wedge. The development of such suprastructure-infrastructure transition zones is commonly associated with thermo-mechanical relaxation of a thickened crust resulting in upward propagating mechanical weakening. Therefore the position of suprastructure-infrastructure transition zone commonly changes through time (Beaumont et al., 2006; Culshaw et al., 2006). In contrast, the Ochtiná Unit represents an unusual example of a suprastructure-infrastructure transition zone with its position being predefined and fixed by the mechanical weakness of this sedimentary horizon.

6.5. Implications for the pre-convergent setting of the Ochtiná sediments

If the Ochtiná Unit represents a tectonic mélange, which formed at the base of the overriding Gemer Unit, it appears rather suspicious that it does not contain rocks of the Gemer cover nor of the overlying subduction-accretionary complex of the Meliata ocean (Faryad and Henjes-Kunst, 1997). A possible explanation of this phenomenon involves the post-Lower Carboniferous evolution of the Ochtiná basin as well as the initial stages of Cretaceous collision.

The previously assumed cover relationship of the Ochtiná metasediments to the Gemer basement is contradicted by the fact that the rocks of the Ochtiná Unit never occur upon the Gemer

basement, which in turn is discordantly overlain by the Upper Carboniferous succession of the Dobšiná group and Permian conglomerates (Kozur et al., 1976; Rakusz, 1932). For this reason some authors proposed the existence of a basin separating the Vepor and Gemer during Late Paleozoic–Mesozoic (e.g., Abonyi, 1971; Kozur and Mock, 1997) and others associate the sediments of the Ochtiná Unit with the Vepor Unit (Németh et al., 2006). Indeed, the geochemical data from phyllites and meta-sandstones presented in this work point to acidic continental arc protolith source, which may be sought in the Vepor basement dominated by Carboniferous granitoids. Furthermore, a recent study of detritic zircons in one meta-sandstone sample from the Ochtiná Unit shows a dominance of Upper Devonian-Carboniferous zircons (Vozárová et al., 2013), which are frequent in the Vepor basement but nearly absent in Gemer (cf. Michalko et al., 1998; Vozárová et al., 2010). Although very little is known about the basin separating the Gemer and Vepor units, it is sometimes considered as a root zone for a thick Mesozoic carbonate sequence preserved in the rootless Choč nappe overriding the Krížna nappe in the northern Vepor and Tatra Units. There is a remarkable stratigraphic coincidence between the Lower Carboniferous metasediments of the Ochtiná Unit and the basal part of the Choč nappe formed by Upper Carboniferous shales and conglomerates. The origin of the Choč nappe in the Ochtiná basin may actually explain the lack of upper crustal rocks in the Ochtiná mélange. As the Cretaceous convergence in the West Carpathians started in the south with the closure of the Ochtiná basin between the Gemer and Vepor blocks, it appears likely that the rheologically weak horizon of the Ochtiná sediments acted as a décollement zone already for the overlying strong carbonate platform of the Upper Carboniferous-Cretaceous deposits of the future Choč sequence. The Choč nappe was thus pushed northwards from its root zone by the thickening

Gemer Unit, however at the same time it served as a lid preventing the Gemer derived debris from getting into the basal thrust zone. This scenario is further supported by the overlap of the recently published ages related to thickening of the Gemer Unit starting at ca. 137 Ma (Hurai et al., 2008; Vozárová et al., 2014) with the youngest Valagian sediments in the the Choč nappe (Jablonský et al., 2001). These sediments comprise chromium-spinel bearing turbidites, which may be associated with denudation of the Meliata accretionary complex overlying the thickening Gemer Unit. This scenario may also explain the lack of the Gemer and Meliata derived debris in the Ochtiná basal thrust zone.

7. Conclusion

1) The Ochtiná Unit is characterized by a complex lithological assemblage of exotic hard blocks, lenticular in shape enclosed in a weak phyllite matrix. Petrological analysis by means of phase equilibrium modelling revealed that the lenses are characterised by contrasting metamorphic histories with peak PT conditions of 500-600 °C and 4-6.5 kbar for amphibolite, and 500-520 °C and 9-11 kbar for chloritoid schist. These PT estimates document two distinct metamorphic field gradients presumably related to Variscan and Alpine metamorphic events, respectively. The heterogeneous lithological and metamorphic record is consistent with a block-in-matrix type of rock assemblage and consequently the Ochtiná Unit is interpreted as deep seated tectonic mélange.

2) The mélange formed during the Cretaceous Eo-Alpine collision at the boundary between two major crustal nappes of the West Carpathians – the Gemer and Vepor Units. The mélange evolved via repeated slip along the rheologically weak sediments of the Ochtiná Unit during the

building and collapse of the Central West Carpathians orogenic wedge. Deformation record indicates that the mélange separates two distinct structural domains marked by a decoupled behaviour, i.e. the orogenic suprastructure represented by the Gemer Unit and infrastructure represented by the Vepor Unit. With this respect, the Ochtiná Unit represents an unusual example of a suprastructure-infrastructure transition zone with its position being controlled by the mechanical weakness of this sedimentary horizon and not by the usual thermal maturation.

3) The lack of the upper crustal rocks derived from the Gemer Unit within the Ochtiná Unit mélange may be explained by the presence of the Mesozoic carbonates of the Choč nappe in the Ochtiná basin prior to the Cretaceous collision.

8. Acknowledgements

This work was supported by the research grants of the Charles University in Prague GAUK 5545/2012 and of the Czech Science Foundation GACR 205/09/1041. Z. Bukovská is thanked for field work participation and V. Janoušek for discussing the geochemical data. A. Festa and D. Plašienka are thanked for constructive reviews, which were helpful in improving this article.

9. References

Abonyi, A., 1971. Stratigraficko-tektonický vývoj karbónu Gemeríd západne od Štítnického

zlomu (In Slovak). Geol. Práce, Správy 57, 339–348.

Abonyi, A., Abonyiová, M., 1981. Magnesite ore deposits of Slovakia (In Slovak). Miner. Slovaca, Monogr., Alfa Bratislava, pp.1-125.

Andrusov, D., 1936. The subtatric nappes in the Western Carpathians (In Slovak). Carpatica 1, 3–50.

Auzanneau, E., Schmidt, M.W., Vielzeuf, D., Connolly, J. A. D., 2010. Titanium in phengite: a geobarometer for high temperature eclogites. Contrib. to Mineral. Petrol. 159, 1–24, doi: 10.1007/s00410-009-0412-7.

Bajaník, Š., 1976. To the petrogenesis of Devonian volcanic rocks of the Spišsko-gemerské rudohorie Mts. - Western Carpathians (In Slovak). Ser. Miner. Petrog. Geoch. Lož. 2, 75–94.

Beaumont, C., Nguyen, M.H., Jamieson, R.A., Ellis, S., 2006. Crustal flow modes in large hot orogens. Geol. Soc. London, Spec. Publ. 268, 91–145, doi: 10.1144/GSL.SP.2006.268.01.05.

Bhatia, M.R., Crook, K.A.W., 1986. Trace element characteristics of greywackes and tectonic setting discrimination of sedimentary basins. Contrib. to Mineral. Petrol. 92, 181–193, doi: 10.1093/petrology/25.4.956.

Bibikova, E. V., Cambel, B., Korikovsky, S.P., Broska, I., Gracheva, T. V., Makarov, V.A., Arakeliants, M., 1988. U-Pb and K-Ar isotopic of Sinec (Rimavica) granites (Kohút zone of Veporides). Geol. Carpathica 39, 147–157.

Bukovská, Z., Jeřábek, P., Lexa, O., Konopásek, J., Janák, M., Košler, J., 2013. Kinematically unrelated C—S fabrics: an Lexample of extensional shear band cleavage from the Veporic Unit (Western Carpathians). Geol. Carpathica 64, 103–116, doi: 10.2478/geoca-2013-0007.

Coggon, R., Holland, T.J.B., Street, D., 2002. Mixing properties of phengitic micas and revised garnet-phengite thermobarometers. J. Metamorph. Geol. 20, 683–696, doi: 10.1046/j.1525-1314.2002.00395.x.

Connolly, J.A.D., 2005. Computation of phase equilibria by linear programming: A tool for geodynamic modeling and its application to subduction zone decarbonation. Earth Planet. Sci. Lett. 236, 1-2, 524-541, doi: 10.1016/j.epsl.2005.04.033.

Culshaw, N.G., Beaumont, C., Jamieson, R.A., 2006. The orogenic superstructure-infrastructure concept: Revisited, quantified, and revived. Geology 34, 733–736, doi: 10.1130/G22793.1.

Dela Pierre, F., Festa, A., Irace, A., 2007. Interaction of tectonic, sedimentary, and diapiric processes in the origin of chaotic sediments: An example from the Messinian of Torino Hill (Tertiary Piedmont Basin, northwestern Italy). Geol. Soc. Am. Bull. 119, 1107–1119, doi:

10.1130/B26072.1.

Diener, J.F. a., Powell, R., 2012. Revised activity-composition models for clinopyroxene and amphibole. J. Metamorph. Geol. 30, 131–142, doi: 10.1111/j.1525-1314.2011.00959.x.

Faryad, S.W., 1990. Gneiss-amphibolite Complex of the Gemericum. Miner. Slovaca 22, 303–318.

Faryad, S.W., 1991a. Pre-alpine metamorphic events in Gemericum. Miner. Slovaca 23, 395–402.

Faryad, S.W., 1991b. Metamorfóza sedimentov staršieho paleozoika gemerika (In Slovak). Miner. Slovaca 23, 315–324.

Faryad, S.W., 1994. Mineralogy of Mn-rich rocks from greenshist facies sequences of the Gemericum, West Carpathians. Neues Jahrb. fur Mineral. 10, 464–480.

Faryad, S.W., 1995. Phase petrology and P-T conditions of mafic blueschists from the Meliata unit, West Carpathians, Slovakia. Journal of Metamorphic Geology. J. Metamorph. Geol. 13, 701–714, doi: 10.1111/j.1525-1314.1995.tb00253.x .

Faryad, S.W., Bernhardt, H.J., 1996. Taramite-bearing metabasites from Rakovec (Gemeric Unit,

The Western Carpathians). Geol. Carpathica 47, 349–357.

Faryad, S.W., Henjes-Kunst, F., 1997. Petrological and K-Ar and 40Ar-39Ar age constraints for the tectonothermal evolution of the high-pressure Meliata unit, Western Carpathians (Slovakia). Tectonophysics 280, 141–156, doi:10.1016/S0040-1951(97)00141-8

Faryad, S.W., 1999. Metamorphic evolution of the eastern part of the Western Carpathians , with emphasis on Meliata Unit. Acta Montan. Slovaca 4, 148–160.

Faryad, S.W., Dianiška, I., 1999. Alpine overprint in the early Paleozoic of the Gemericum. Miner. Slovaca 31, 485-490.

Festa, A., Pini, G.A., Dilek, Y., Codegone, G., 2010. Mélanges and mélange-forming processes: a historical overview and new concepts. Int. Geol. Rev. 52, 1040–1105, doi: 10.1080/00206810903557704.

Festa, A., Dilek, Y., Pini, G.A., Codegone, G., Ogata, K., 2012, Mechanisms and processes of stratal disruption and mixing in the development of mélanges and broken formations: Redefining and classifying mélanges. Tectonophysics, v. 568-569, p. 7-24, doi:10.1016/j.tecto.2012.05.021.

Floyd, P.A., Leveridge, B.E., 1987. Tectonic environment of the Devonian Gramscatho basin, south Cornwall: framework mode and geochemical evidence from turbiditic sandstones. J. Geol.

Soc. London. 144, 531–542, doi: 10.1144/gsjgs.144.4.0531.

Froitzheim, N., Plašienka, D., Schuster, R., 2008. Alpine tectonics of the Alps and Western Carpathians. The geology of Central Europe, 2, 1141-1232.

Grecula, P., 1982. Gemericum - Segment of the Paleotethyan riftogenous basin. Miner. Slovaca-Monogr., Alfa Bratislava, pp.1-263.

Grecula, P., Kobulský, J., Gazdačko, Ľ., Németh, Z., Hraško, Ľ., Novotný, L., Maglay, J., 2009. Geological map of the Spiš-Gemer Ore Mts. at a scale 1:50 000. Bratislava, State geological Institute of Dionýz Štúr.

Holland, T.J.B., Powell, R., 1998. An internally consistent thermodynamic data set for phases of petrological interest. J. Metamorph. Geol. 16, 309–343, doi:10.1111/j.1525-1314.1998.00140.x.

Holland, T., Powell, R., 2003. Activity composition relations for phases in petrological calculations: an asymmetric multicomponent formulation. Contrib. to Mineral. Petrol. 145, 4, 492-501, doi: 10.1007/s00410-003-0464-z.

Hoschek, G., 2004. Comparison of calculated P-T pseudosections for a kyanite eclogite from the Tauern Window, Eastern Alps, Austria. Eur. J. Mineral. 16, 59–72, doi: 10.1127/0935-1221/2004/0016-0059.

Hoschek, G., 2013. Garnet zonation in metapelitic schists from the Eclogite Zone, Tauern Window, Austria: comparison of observed and calculated profiles. Eur. J. Mineral. 25, 615–629, doi: 10.1127/0935-1221/2013/0025-2310.

Hovorka, D., Zlocha, J., 1974. Tectonics and origin of ultrabasic bodies of the Gemeride Mesozoic (West Carpathians). Sbor. geol. Věd 26, 185–193.

Hovorka, D., Ivan, P., 1985. Meta-ultrabasites in the Inner Western Carpathians: Implication for the reconstruction of the tectonic evolution of the region. Ofiolity 10, 317–328.

Hovorka, D., Ivan, P., Méres, Š., 1997. Leptyno-amphibolite complex of the Western Carpathians: Its definition, extent and genetical problems., in: Grecula, P., Putiš, D., Hovorka, M. (Eds.), Geological Evolution of the Western Carpathians. Miner. Slovaca-Monograf., Bratislava, pp. 269–280.

Huang, C.Y., Chien, C.W., Yao, B., Chang, C.P., 2008. The Lichi Mélange: A collision mélange formation along early arcward backthrusts during forearc basin closure, Taiwan arc-continent collision. Geol. Soc. Am. Spec. Pap. 436, 127–154, doi: 10.1130/2008.2436(06)

.

Hurai, V., Prochaska, W., Lexa, O., Schulmann, K., Thomas, R., Ivan, P., 2008. High-density nitrogen inclusions in barite from a giant siderite vein: implications for Alpine evolution of the

Variscan basement of Western Carpathians, Slovakia. J. Metam. Geol., 26,4, 487-498, doi: 10.1111/j.1525-1314.2008.00775.x

Hurai, V., Huraiová, M., Koděra, P., Prochaska, W., Vozárová, A., Dianiška, I., 2011. Fluid inclusion and stable CO isotope constraints on the origin of metasomatic magnesite deposits of the Western Carpathians, Slovakia. Russ. Geol. Geophys. 52, 1474–1490, doi: 10.1016/j.rgg.2011.10.015.

Chang, C.P., Angelier, J., Huang, C.Y., Liu, C.S., 2001. Structural evolution and significance of a mélange in a collision belt: the Lichi Mélange and the Taiwan arc–continent collision. Geol. Mag. 138, 633–651, doi: 10.1017/S0016756801005970.

Ivan, P., 2008. Staropaleozoický bázický vulkanizmus Západných Karpát: Geochémie a geodynamická pozícia. Acta Geologica Universitatis Comenianae, Bratislava, pp. 1-94.

Jablonský, J., Sýkora, M., Aubrecht, R., 2001. Detritic Cr-spinels in Mesozoic sedimentary rocks of the Western Carpathians (overview of the latest knowledge. Miner. Slovaca, 33, 487-498.

Janák, M., Plašienka, D., Frey, M., Cosca, M., Schmidt, S.T., Lupták, B., Méres, Š., 2001. Cretaceous evolution of a metamorphic core complex, the Veporic unit, Western Carpathians (Slovakia): P–T conditions and in situ40Ar/39Ar UV laser probe dating of metapelites. J. Metamorph. Geol. 19, 197–216, doi: 10.1046/j.0263-4929.2000.00304.x

Janoušek, V., Farrow, C.M., Erban, V., 2006. Interpretation of whole-rock geochemical data in igneous geochemistry: introducing Geochemical Data Toolkit (GCDkit). J. Petrol. 47, 1255–1259, doi: 10.1093/petrology/egl013

Jeřábek, P., Stünitz, H., Heilbronner, R., Lexa, O., Schulmann, K., 2007. Microstructural-deformation record of an orogen-parallel extension in the Vepor Unit, West Carpathians. J. Struct. Geol. 29, 1722–1743, doi: 10.1016/j.jsg.2007.09.002.

Jeřábek, P., Faryad, S.W., Schulmann, K., Lexa, O., Tajčmanová, L., 2008. Alpine burial and heterogeneous exhumation of Variscan crust in the West Carpathians; insight from thermodynamic and argon diffusion modelling. J. Geological Soc. 165, 479–498, doi: 10.1144/0016-76492006-165

Jeřábek, P., Lexa, O., Schulmann, K., Plašienka, D., 2012. Inverse ductile thinning via lower crustal flow and fold-induced doming in the West Carpathian Eo-Alpine collisional wedge. Tectonics 31, 5, 1-26, doi: 10.1029/2012TC003097.

Klinec, A., 1966. On the structure and evolution of the Veporic crystalline unit. Geol. Zborník 6, 7–28.

Kozur, H., Mock, R., Mostler, H., 1976. Stratigraphische Neue-instufung der Karbonategesteine

der unteren Schichtenfolge von Ochtiná (Slovakei) in das oberste Vise Serpukchovian (Namur A). Geol. Paläont. Mitt. 6, 1–29.

Kozur, H., Mock, R., 1997. New paleogeographic and tectonic interpretations in the Slovakian Carpathians and their implications for correlations with the Eastern Alps and other parts in the Western Tethys. Part II. Inner Western Carpathians. Miner. Slovaca 29, 164–209.

Leake, B.E., Woolley, A.R., Birch, W.D., Burke, E.A., Ferraris, G., Grice, J.D., Whittaker, E.J., 1997. Nomenclature of amphiboles: additions and revisions to the International Mineralogical Association's 1997 recommendations. Can. Mineral. 41, 1355–1362, doi: 10.2113/gscanmin.41.6.1355.

Lexa, O., Schulmann, K., Ježek, J., 2003. Cretaceous collision and indentation in the West Carpathians: View based on structural analysis and numerical modeling. Tectonics 22, 6, 1–16, doi: 10.1029/2002TC001472.

López-Carmona , A., A., Pitra, P., Abati, J., 2013. Blueschist-facies metapelites from the Malpica–Tui Unit (NW Iberian Massif): phase equilibria modelling and H2O and Fe2O3 influence in high-pressure assemblages. Journal of Metamorphic Geology, 31, 3, 263-280, doi: 10.1111/jmg.12018.

Lupták, B., Janák, M., Plašienka, D., Schmidt, S.T., Frey, M., 2000. Chloritoid-kyanite schists

from the Veporic unit, Western Carpathians, Slovakia: implications for Alpine (Cretaceous) metamorphism. Schweizerische Mineral. und Petrol. Mitteilungen 80, 213–223.

Lupták, B., Janák, M., Plašienka, D., Schmidt, S.T., 2003. Alpine low grade metamorphism of the Permian-Triassic sedimentary rocks from the Veporic superunit, Western Carpathians: phyllosilicate composition and „crystallinity“ data. Geol. Carpathica 54, 367–375.

Matějka, A., Andrusov, D., 1931. Apercu de la geologic des Garpates occidentales de la Slovaquie centrale et des regions avoisinantes. Knihovna Státního Geologického Ústavu ČSR, Praha, pp. 19–136.

Michalko, J., Bezák, V., Hraško, Ľ., 1998. U/Pb zircon data from the Veporic granitoids (Western Carpathians). Krystalinikum 24, 91–104.

Mock R., Sýkora M., Aubrecht R., Ožvoldová L., Kronome B., Reichwalder P., Jablonský J., 1998: Petrology and stratigraphy of the Meliaticum near the Meliata and Jaklovce Villages, Slovakia. Slovak Geol. Mag., 4, 223–260.

Němejc, F., 1946. Further critical remarks on Sternberg’s Lepidodendron dichotomum and its relations to the cones of Sporangiostrobus Bode. Rozpr. II. třídy České Akad. Věd 47, 7, 1-11.

Németh, Z., Radvanec, M., Hraško, Ľ., Madarás, J., 2006. Ochtinská zóna z pohľadu nových výsledkov mapovacieho a petrologického výskumu v stykovej zóne veporika a gemerika. Geol. práce, Správy 15.

Neubauer, F., Vozárová, A., 1990. The Noetsch-Veitsch-North gemeric zone of the Alps and Carpathians: Correlation, paleogeography and significance for Variscan orogeny., in: Thirty Years of Geological Coooperation Between Austria and Czechoslovakia, Ústr. Ústav geologický, Praha, pp. 167–171.

Pearce, J.A., Norry, M.J., 1979. Petrogenetic implications of Ti, Zr, Y and Nb variations in volcanic rocks. Contrib. to Mineral. Petrol. 69, 1, 33–47, doi: 10.1007/BF00375192.

Planderová, E., Vozárová, A., 1978. Upper Carboniferous in the Souther part of Veporic Unit. Geol. práce, Správy 70, 129–141.

Plašienka, D., Grecula, P., Putiš, M., Kováč, M., Hovorka, D., 1997. Evolution and structure of the Western Carpathians: an overview, in: Grecula, P., Hovorka, D., Putiš, M. (Eds.), Geological Evolution of the Western Carpathians. Miner. Slovaca, Bratislava, p. 1-24.

Plašienka, D., Janák, M., Lupták, B., Milovský, R., Frey, M., 1999. Kinematics and metamorphism of a cretaceous core complex: The veporic unit of the Western Carpathians. Phys. Chem. Earth, Part A: Solid Earth Geod. 24, 8, 651-658, doi: 10.1016/S1464-1895(99)00095-2.

Plašienka, D., Soták, J., 2001. Stratigraphic and tectonic position of Carboniferous sediments in the Furmanec valley (Muránska planina). Miner. Slovaca 33, 29–44.

Plašienka, D., 2003. Development of basement-involved fold and thrust structures exemplified by the Tatric–Fatric–Veporic nappe system of the Western Carpathians (Slovakia). Geodinamica Acta, 16,1, 21-38, doi: 10.1016/S0985-3111(02)00003-7.

Poller, U., Uher, P., Broska, I., Plašienka, D., Janák, M., 2002. First Permian–Early Triassic zircon ages for tin-bearing granites from the Gemeric unit (Western Carpathians, Slovakia): connection to the post-collisional extension of the Variscan orogen and S-type granite magmatism. Terra Nov. 14, 1, 41–48, doi: 10.1046/j.1365-3121.2002.00385.x.

Powell, R., Holland, T.J.B., 1988. An internally consistent dataset with uncertainties and correlations: 3. Applications to geobarometry, worked examples and a computer program. J. Metamorph. Geol. 6, 2, 173–204, doi: 10.1111/j.1525-1314.1988.tb00415.x.

Prochaska, W., 2000. Magnesite and talc deposits in Austria. Miner. Slovaca 32, 6, 543–548.

Prokešová R., Plašienka D., Milovský R., 2012: Structural pattern and emplacement mechanisms of the Krížna cover nappe (Western Carpathians, Slovakia). Geologica Carpathica, 63, 1, 13–32. doi: 10.2478/v10096-012-0001-y

Rakusz, G., 1932. Die Oberkarbonischen Fossilien von Dobsina (Dobišina) und Nagyisnyó. Inst. Regni Hungariae Geologicum, Geologica Hungarica, 8.

Ratschbacher, L., 1986. Kinematics of Austro-Alpine cover nappes: changing translation path due to transpression. Tectonophysics 124, 4, 335–356, doi: 10.1016/0040-1951(86)90170-8.

Raymond, L.A., 1984. Classification of melanges. In: Raymond, L.A. (Ed.), Melanges: Their nature, origin and significance. Boulder, Colorado. Geological Society of America Special Papers 198, 7-20.

Roser, B.P., Cooper, R.A., Nathan, S., Tulloch, A.J., 1996. Reconnaissance sandstone geochemistry, provenance, and tectonic setting of the lower Paleozoic terranes of the West Coast and Nelson, New Zealand. New Zeal. J. Geol. Geophys. 39, 1, 1-16, doi: 10.1080/00288306.1996.9514690.

Rozlozsnik, P., 1935. Die Geologische Verhältnisse der gegend von Dobšiná. Geologica Hungarica, Ser. Geol 5, 1-118.

Rudnick, R.L., Gao, S., 2003. The composition of the continental crust, in: The Crust. Elsevier-Pergamon, Oxford, 1–64, doi:10.1016/B0-08-043751-6/03016-4.

Silver, E.A., Beutner, E.C., 1980. Melanges. Geology 8, 32-34.

Šucha, V., Eberl, D.D., 1992. Burial metamorphism of the Permian sediments from the Western Carpathians. Miner. Slovaca 24, 399–405.

Tomek Č., 1993: Deep crustal structure beneath the central and inner West Carpathians. Tectonophysics, 226, 417–431.

Vozárová, A., 1990. Development of metamorphism in the Gemeric/Veporic contact zone (Western Carpathians). Geol. Carpathica 41, 5, 475–502.

Vozárová, A., 1996. Tectono-sedimentary evolution of Late Paleozoic basins based on interpretation of lithostratigraphic data (Western Carpathians, Slovakia). Slovak Geol. Mag, 3-4.

Vozárová, A., 1998. Hercynian development of the external-Gemeric zone., in: Rakús, M. (Ed.), Geodynamic Development of the Western Carpathians. Dionýz Štúr Publication, Bratislava, 47–61.

Vozárová, A., Šarinová, K., Larionov, A., Presnyakov, S., Sergeev, S., 2010. Late Cambrian/Ordovician magmatic arc type volcanism in the Southern Gemericum basement, Western Carpathians, Slovakia: U–Pb (SHRIMP) data from zircons. Int. J. Earth Sci. 99, 1, 17–37, doi: 10.1007/s00531-009-0454-0.

Vozárová, A., Laurinc, D., Šarinová, K., Larionov, A., Presnyakov, S., Rodionov, N., Paderin, I., 2013. Pb ages of detrital zircons in relation to geodynamic evolution: Paleozoic of the Northern Gemericum (Western Carpathians, Slovakia). J. Sediment. Res. 83, 11, 915–927.

Vozárová, A., Konečný, P., Šarinová, K., & Vozár, J. (2014). Ordovician and Cretaceous tectonothermal history of the Southern Gemericum Unit from microprobe monazite geochronology (Western Carpathians, Slovakia).International Journal of Earth Sciences, 103(4), 1005-1022, doi: 10.1007/s00531-014-1009-6

Vrána, S., 1964. Chloritoid and kyanite zone of alpine metamorphism on the boundary of the Gemerides and the Veporides (Slovakia). Krystalinikum 2, 125–143.

White, R.W., Powell, R., Holland, T.J.B., 2007. Progress relating to calculation of partial melting equilibria for metapelites. J. Metamorph. Geol. 25, 5, 511–527, doi: 10.1111/j.1525-1314.2007.00711.x.

White, R.W., Powell, R., Holland, T.J.B., Worley, B.A., 2000. The effect of TiO2 and Fe2O3 on metapelitic assemblages at greenschist and amphibolite facies conditions: mineral equilibria calculations in the system K2O-FeO-MgO-Al2O3-SiO2- H2O-TiO2-Fe2O3. J. Metamorph. Geol. 18, 5, 497–511, doi: 10.1046/j.1525-1314.2000.00269.x.

Winchester, J.A., Floyd, P.A., 1977. Geochemical discrimination of different magma series and their differentiation products using immobile elements. Chem. Geol. 20, 325-343, doi: 10.1016/0009-2541(77)90057-2.

Wood, D.A., 1980. The application of a ThHfTa diagram to problems of tectonomagmatic classification and to establishing the nature of crustal contamination of basaltic lavas of the British Tertiary Volcanic Province. Earth Planet. Sci. Lett. 50, 1, 11-30, doi: 10.1016/0012-821X(80)90116-8.

10. Figure captions

Fig. 1: (a) Simplified geological map of Slovakia with the major units and nappes. (b) Lithotectonic map of the Gemer-Vepor Contact Zone and surrounding units with location of studied samples. Inset in b corresponds to figure 2b.

Fig. 2: (a) Pole figures (lower hemisphere, equal-area Schmidt projection) of documented deformation structures. For the structural measurements, solid symbols corespond to the ENE-WSW-trending part of the belt and open symbols to the NNE-SSW-trending part. (b) Detailed lithological and structural map of the selected area in the Gemer-Vepor Contact Zone (see figure 1 for location). Map based on the Gelogical map of the Slovak Rebublic, 1:50 000 http://mapserver.geology.sk. (c) Detailed NW-SE trending gelogical-structural cross section across the Gemer-Vepor Contract Zone.

Fig. 3: (a) Micrograph of the Vepor basement schist showing the relationship between the S_V

assemblage represented by relic cores of garnets, biotite porphyroblasts and plagioclase being overprinted by S_{A1} fabric represented by garnet rims, biotite(II), albite, epidote and white mica (locality: Blh-Krokávka). (b) Micrograph of the Vepor basement schist with the relationship between S_{A1} and S_{A2} fabrics. S_{A1} is associated with newly formed garnet(II). Muscovite- and chlorite-bearing cleavage S_{A2} subsequently folds and overprints S_{A1} (locality: Krokávka, S_{A2}~ 182/30). (c) Field photograph from the Vepor metasedimentary cover with the higher grade fabric S_{A1} being overprinted by the lower grade cleavage S_{A2} (locality: Hanková- Klihov). (d) Micrograph of the Ochtiná Unit phyllite showing overprint of the S_{A1} fabric-represented mainly by the distinct quartz microstructure- by the lower grade cleavage S_{A2} represented by muscovite, chlorite and graphite (locality: Nižná Burda, S_{A2}~ 150/55). (e) Field photograph from the Ochtiná Unit with S_{A1} fabric being folded in association with the S_{A2} cleavage development (locality: Ploské-Ratková). (f) Steep S_{A3} cleavage developed due to the Trans-Gemer Shear Zone formation in the Ochtiná Unit (locality: Hrančiarská ves). Mineral abbreviations are after Holland and Powell, 1998.

Fig. 4: Source rock and tectonic setting discrimination diagrams for the phyllites from Ochtiná Unit. The Upper Continental Crust standard (UCC; Rudnick and Gao, 2003) is plotted for comparism: (a) La/Th vs. Hf diagram (after Floyd and Leveridge, 1987), indicating mixing of felsic and intermediate sources with minor influence of an old sediment component, (b) Ti/Zr vs La/Sc diagram (after Bhatia and Crook, 1986), (c) triangular trace element tectonic discrimination diagram (Bhatia and Crook, 1986).

Fig. 5: Back Scattered Electron (BSE) images from chloritoid sample NN155 (a-c) and

amphibolite sample NN25 (d-f). (a) BSE image of radial chloritoid spherulites. (b) Element distribution map of iron demonstrating lack of chemical zoning in chloritoid. (c) BSE image showing the relationship of muscovite and paragonite. The paragonite intergrows with muscovite in a close vicinity of chloritoid. (d) BSE image showing zoned calcic clinoamphiboles, epidote and plagioclase matrix and chlorite present in micro shear zones cross-cutting the amphibole porphyroblast. (e) BSE image of relic oligoclase overgrown by albite. (f) Element distribution map of Al showing the amphibole zonation and the cores of actinolite composition rimmed by hornblende.

Fig. 6: Classification diagram for calcic clinoamphiboles after IMA (International Mineralogical Association, Leake et al., 1997) from the Ochtiná amphibolites samples NN25, NN57 and NN136. For representative analyses of amphibole see Table 2

Fig. 7: (a) Zr-Ti vs. SiO_2 discrimination diagram (after Winchester and Floyd, 1977). (b) Classification provided by the Th-Hf/3-Ta discrimination diagram (Wood, 1980). (c) Zr/Y vs. Zr diagram for basic rocks (after Pearce and Norry, 1979). The previously published data from amphibolites of the Gemer basement (Bajaník, 1976; Ivan, 2008) are shown for comparison in (a-c). The Geochemical Data Toolkit (GCDkit, Janoušek et al., 2006) was used to create these diagrams. Abbreviations: MORB= middle ocean ridge basalt.

Fig. 8: (a) Micrograph of the serpentinite, showing the randomly oriented serpentine and the talc, magnetite and chlorite filling the fractures. (b) Micrograph of the actinolite schist. Prismatic crystals of actinolite which are in some cases parallel to the foliation and in some they show variable orientation.

Fig. 9: P-T pseudosection for chloritoid schist sample NN155 with compositional isopleths of X_{Mg} in chloritoid and Si in muscovite. Resulting P-T conditions are highlighted by pinkish polygon. The section was calculated in the MnNKFMASHTO system using the Perple_X v. 6.6.8 with quartz and water in excess. The bulk rock composition in molar proportion is indicated above the section.

Fig. 10: P-T pseudosection for amphibolite sample NN25 with compositional isopleths of XAl(M2) in hornblende and X_{Ca} in plagioclase. Resulting P-T conditions are highlighted by the pink polygon. The section was calculated in the NCFMASHTO system using THERMOCALC v. 3.33. The bulk rock composition in molar proportion is indicated above the section.

Fig. 11: P-X_O pseudosection calculated at 520° C for NN25. X_O corresponds to the amount of Fe_2O_3. The modeled values in P-T section for X_{Ca} in plagioclase start at the value of ca. 0.20 (Fig. 10), this does not correspond to the analyzed values. The P-X section was constructed to check, whether this may be influenced by the actual Fe_2O_3/FeO ratio. Even at very low values of Fe_2O_3 the proportion of anorthite in plagioclase does not reach values lower than 0.2.

Fig. 12: Summary P-T diagram showing P-T estimates for chloritoid schist sample NN155 (Fig. 9) and amphibolite sample NN25 (Fig. 10) as well as selected published P-T data from Gemer and Vepor Units (Faryad and Bernhardt, 1996; Faryad and Dianiška, 1999; Faryad, 1995, 1991a, 1991b; Janák et al., 2001; Jeřábek et al., 2008), where the middle calculated values were plotted. The data for the Ochtiná Unit samples reveal two contrasting metamoprhic field gradients for Variscan and Alpine metamorphism. The metamorphic field gradients are after Jeřábek et al., 2008 derived for Vepor Unit.

Fig. 13: Proposed model of Ochtiná mélange evolution during the D_{A1}, D_{A2} and D_{A3} deformational phases (see text). The amphibolites samples are in red (NN25 and NN57), the chloritoid schist (NN155) is in blue. (a)D_{A1} phase, the Gemer Unit is thrusting over the Vepor Unit, which leads to its burial. (b) D_{A2} phase, subsequent exhumation and unroofing of Vepor Unit, (c) DA3 phase Trans-Gemer Shear Zone (TGSZ) formation due to thetranspressional lateral escape of Gemer Unit.

11. Table captions

Tab. 1: Whole rock analyses of phyllite, chloritoid schist and amphibolite from the Ochtiná Nappe. Values are given in wt. %.

Sample	NN 123	NN 135	NN 142	R 40	TU 5	NN155	UCC	Sample	NN 123	NN 135	NN 142	R 40	TU 5	NN155	UCC
SiO_2	51,16	69,83	65,19	71,30	58,58	66,95	66,60	Y	23,8	13,5	27,4	27,9	32,7	40	21
Al_2O_3	14,24	13,54	22,20	13,62	21,35	16,95	15,40	La	26,1	17,1	31,9	38,5	40,5		31
Fe_2O_3	7,98	5,10	2,27	2,21	6,52	8,27	5,40	Ce	55,6	33,2	79,7	78,8	78,8		63
MgO	5,06	2,21	0,35	0,68	1,49	1,34	2,48	Pr	6,47	3,59	8,44	8,78	10,92		7,1
CaO	7,10	0,17	0,07	2,07	0,19	0,04	3,59	Nd	23,9	12,2	27,9	31	40,5		27
Na_2O	2,61	2,44	2,06	2,04	0,91	0,62	3,27	Sm	4,95	2,31	5,48	5,75	8,03		4,7
K_2O	1,24	2,28	3,34	4,23	4,10	1,50	2,80	Eu	1,30	0,55	1,20	1,03	1,74		1
TiO_2	1,42	0,63	0,73	0,26	0,97	0,90	0,64	Gd	4,80	2,24	5,13	5,28	7,31		4
P_2O_5	0,29	0,12	0,02	0,06	0,07	0,06	0,15	Tb	0,76	0,38	0,80	0,83	1,08		0,7
MnO	0,14	0,04	0,03	0,05	0,04	0,06	0,10	Dy	4,20	2,51	4,83	4,80	6,06		3,9
Cr_2O_3	0,04	0,01	0,02	0,01	0,02	0,02		Ho	0,85	0,51	1,04	1,02	1,21		0,83
								Er	2,59	1,68	2,86	2,99	3,74		2,3
Ni	120	<20	32	22	41	63	47	Tm	0,37	0,22	0,46	0,42	0,52		0,3
Sc	20	10	15	7	21	17	14	Yb	2,20	1,48	3,17	2,82	3,65		2
Ba	349	619	810	519	720	439	628	Lu	0,34	0,26	0,50	0,44	0,52		0,31
Be	3	3	6	6	12			Cr							92
Co	29,4	6,1	9,1	4,8	10,2			Mo	0,5	0,3	0,2	0,2	0,4		
Cs	1,1	2,3	6,5	3	5,7		4,9	Cu	50,3	22,1	11,4	4,1	32,9		28
Ga	16	14,5	23,6	14,8	23		17,5	Pb	3,4	2,4	3,6	2,2	3,2		17
Hf	4,4	5,6	5,4	2,9	5,6		5,3	Zn	61	50	19	4	70		67
Nb	21,2	9,7	14,7	9,5	13,8	11	12	Ni	103,8	19,7	12,7	7,1	39,5		
Rb	31,8	67,7	143,4	120,8	162,1		82	As	15,8	43,6	14,3	2,8	29,8		
Sn	2	2	4	2	3			Cd	0,1	<0,1	<0,1	<0,1	<0,1		
Sr	223,9	39,4	260,8	25,3	114,3	68	320	Sb	0,2	0,4	<0,1	0,3	0,4		

Ta	1,3	0,7	1,2	0,9	1,1		0,9	**Bi**	<0,1	<0,1	0,5	<0,1	0,6
Th	5,9	9,3	14,8	14,8	15		10,5	**Ag**	<0,1	<0,1	<0,1	<0,1	<0,1
U	1,8	2	2,9	2,6	5,8		2,7	**Au**	3,2	<0,5	35,6	<0,5	3,6
V	174	80	64	31	126		97	**Hg**	<0,01	0,01	<0,01	0,01	0,02
W	0,7	0,9	1,9	2,2	2,3			**Tl**	<0,1	<0,1	<0,1	<0,1	0,1
Zr	170,1	223	188,9	116,1	220,9	325	193	**Se**	<0,5	<0,5	<0,5	<0,5	<0,5

Tab. 2: Representative chemical analyses of selected minerals.

	Apmhibolites				**Ctd schists**				
Analysis	Hb2	Act2	Ab5	Ep5	Chl6	Ctd13	Chl2	Mu11	Mu8
Mineral	**hb**	**act**	**pl**	**ep**	**chl**	**ctd**	**chl**	**mu**	**pa**
SiO_2	42,71	52,56	65,86	37,79	23,81	23,48	23,77	46,48	45,34
TiO_2	0,36	0,06	0,00	0,13	0,00	0,00	0,00	0,17	0,00
Al_2O_3	14,34	3,83	21,44	26,74	40,47	40,44	21,96	36,35	40,00
Cr_2O_3	0,01	0,02	0,00	0,00	0,00	0,00	0,00	0,00	0,00
Fe_2O_3	0,52	0,15	0,00	6,80	1,10	1,92	0,08	0,00	0,00
FeO	16,56	13,98	0,00	1,37	24,16	23,74	30,82	1,44	0,56
MnO	0,24	0,27	0,00	0,13	0,27	0,26	0,27	0,00	0,00
MgO	7,89	13,99	0,00	0,21	2,27	2,28	10,82	0,69	0,00
CaO	11,79	12,82	2,38	23,45	0,00	0,00	0,00	0,00	0,29
Na_2O	1,55	0,46	10,16	0,03	0,00	0,00	0,00	1,31	6,83
K_2O	0,41	0,12	0,10	0,00	0,00	0,00	0,00	8,98	1,20
Totals	**96,38**	**98,26**	**99,95**	**96,64**	**87,18**	**92,07**	**87,72**	**95,42**	**94,21**
Oxygen equivalents	**23**	**23**	**8**	**12,5**	**14**	**6**	**14**	**11**	**11**
Si	6,46	7,59	2,89	3,00	2,68	0,99	2,59	3,07	2,94
Ti	0,04	0,01	0,00	0,01	0,00	0,00	0,00	0,01	0,00
Al	2,56	0,65	1,11	2,50	2,63	1,99	2,82	2,83	3,06
Cr	0,00	0,00	0,00	0,00	0,00	0,00	0,00	0,00	0,00
Fe^{3+}	0,06	0,02	0,00	0,41	0,01	0,03	0,01	0,00	0,00
Fe^{2+}	2,09	1,69	0,00	0,09	2,18	0,84	2,81	0,08	0,03
Mn	0,03	0,03	0,00	0,01	0,03	0,01	0,03	0,00	0,00
Mg	1,78	3,01	0,00	0,03	2,45	0,14	1,76	0,07	0,00
Ca	1,91	1,99	0,11	1,99	0,01	0,00	0,00	0,00	0,02
Na	0,45	0,13	0,87	0,01	0,00	0,00	0,00	0,17	0,86
K	0,08	0,02	0,01	0,00	0,00	0,00	0,00	0,76	0,10
Sum	**15,48**	**15,15**	**4,99**	**8,04**	**9,99**	**4,00**	**10,00**	**6,97**	**7,01**
X_{Mg}	0,46	0,64			0,53	0,14	0,38		
XAl_{M2}	0,51	0,12							
XNa_A	0,40	0,12							

XNa_{M4}	0,05	0,01					
X_{Ca}			0,11				
X_{Fe3+}				0,14			
X_{Na}						0,13	0,85

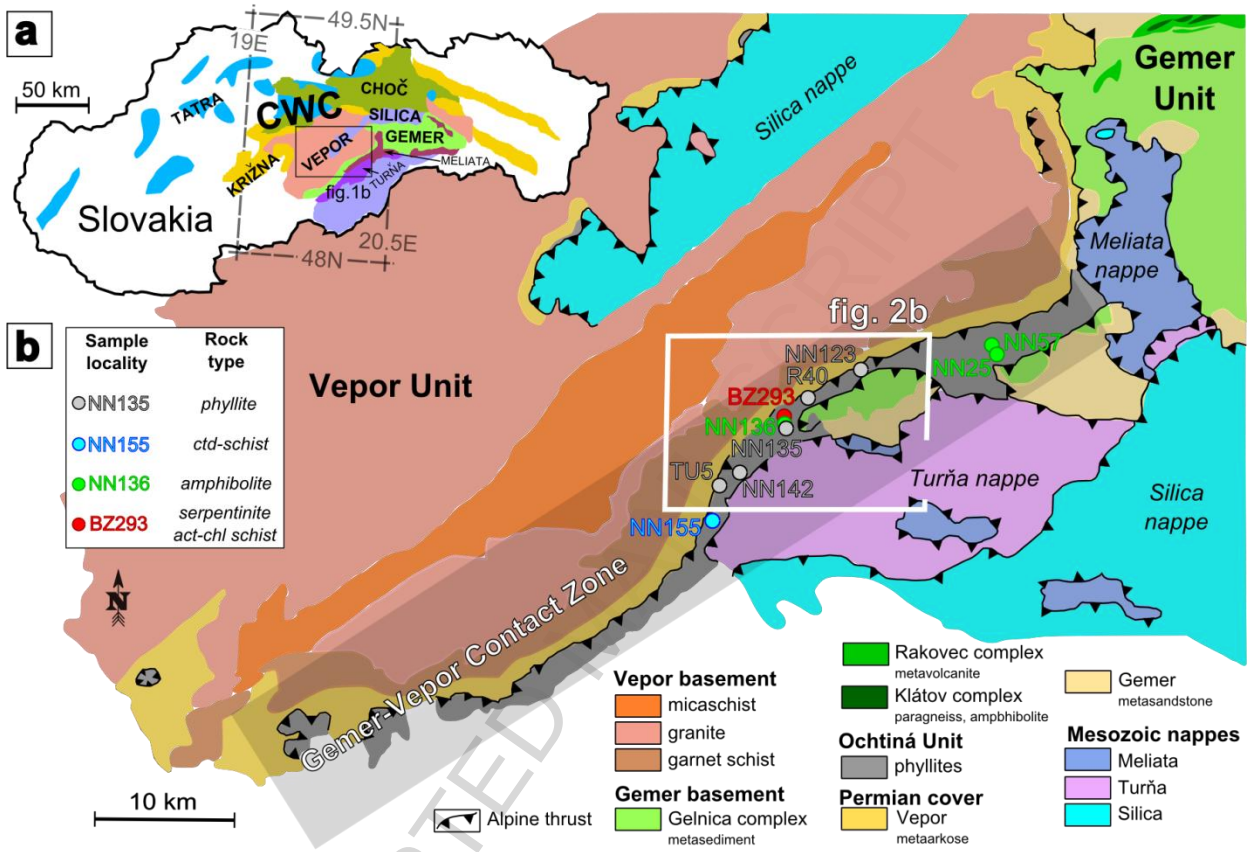

Figure 1

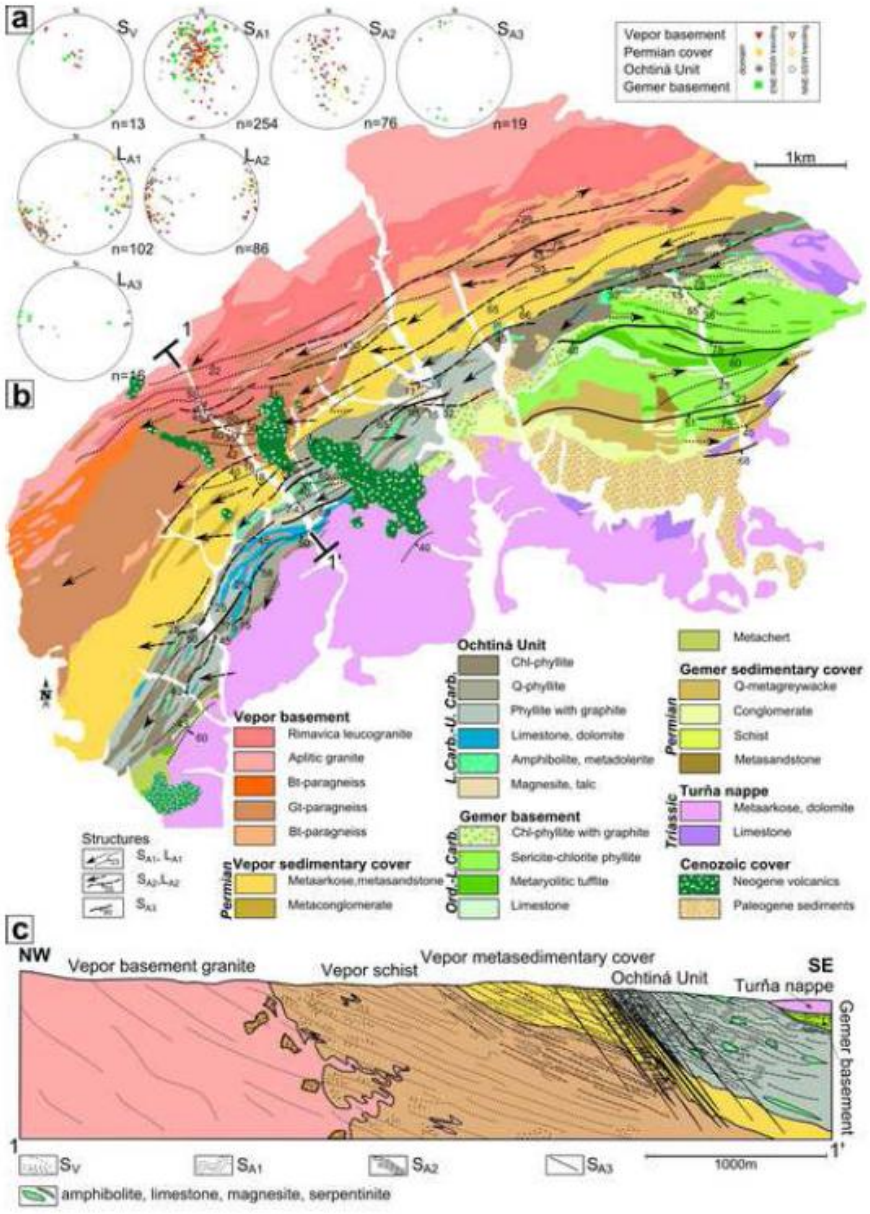

Figure 2

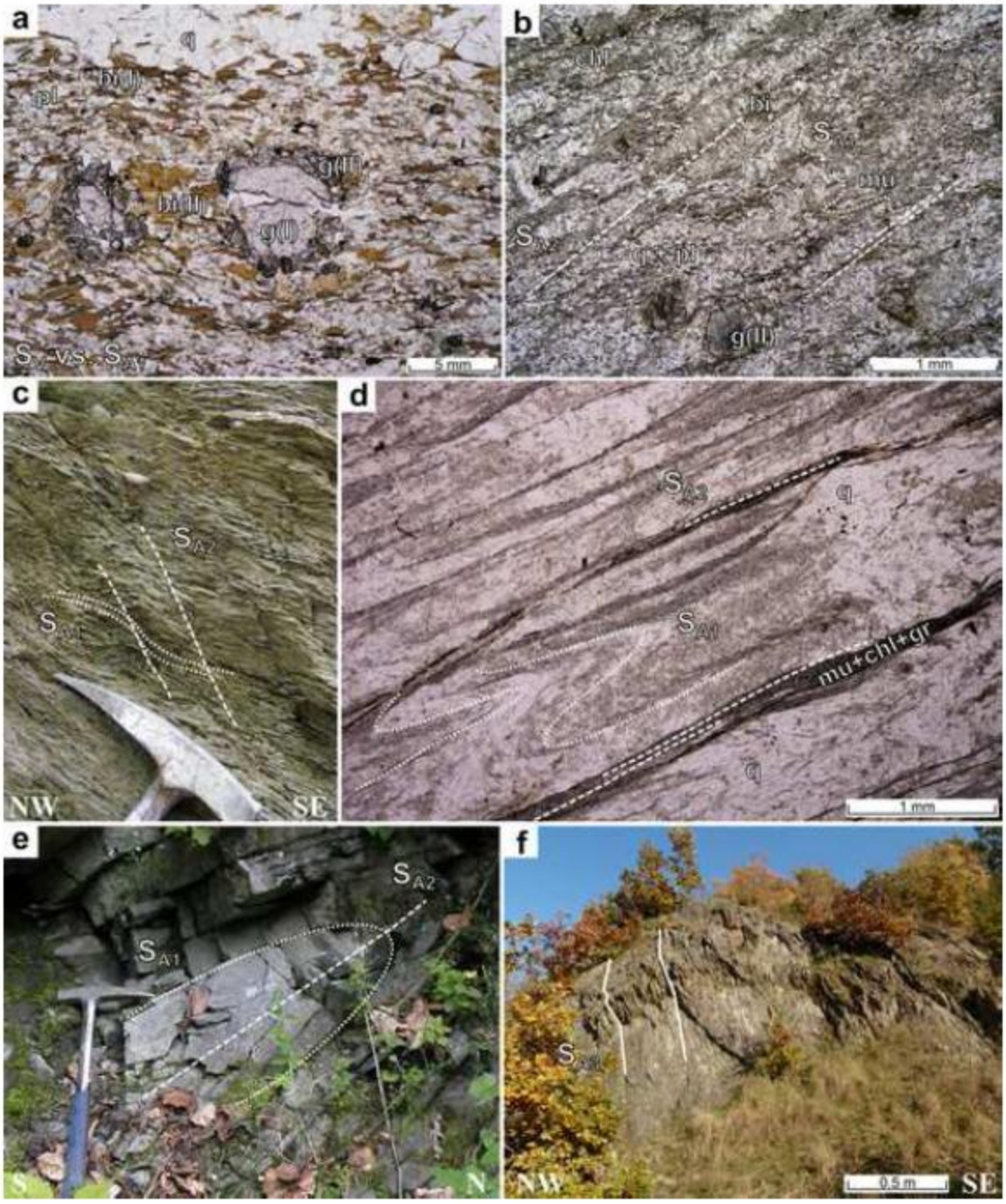
a
q
pl
bi(II)
g(II)
bi(II)
g(II)
S
vs
S
5 mm
b
chl
bi
S
chl
S
bi
g(II)
1 mm
c
S
S
NW
SE
d
S
q
S
mu+chl+gr
q
1 mm
e
S
S
S
N
f
S
NW
0.5 m
SE

Figure 3

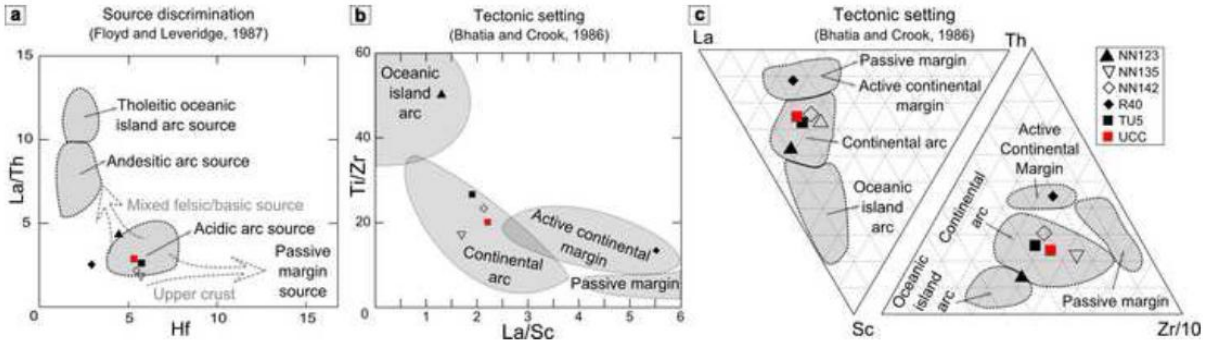

Figure 4

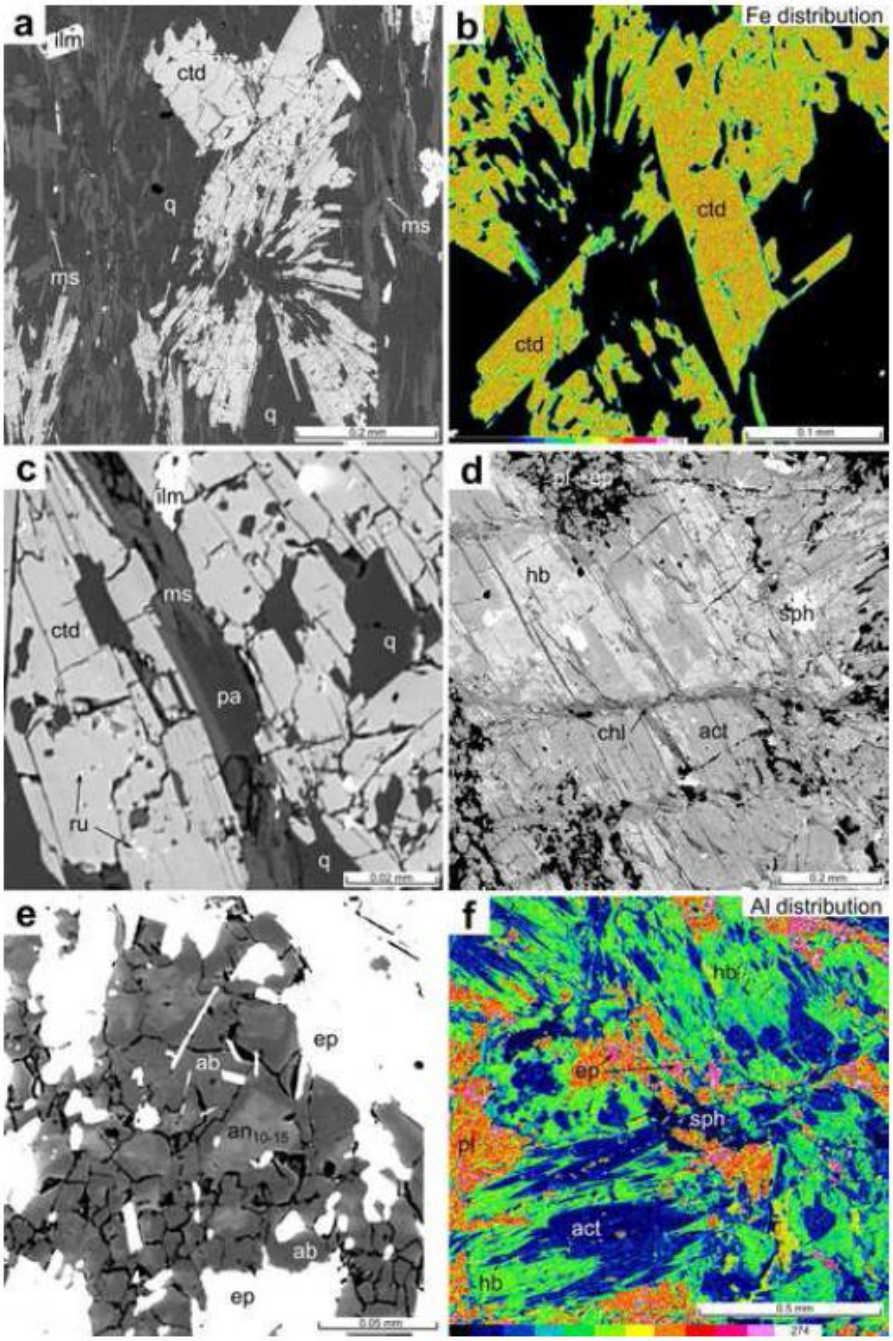
a
ilm
ctd
q
ms
ms
q
b
Fe distribution
ctd
ctd
c
ilm
ms
ctd
q
pa
ru
q
d
hb
sph
chl
act
e
ep
ab
an10-15
ab
ep
f
Al distribution
hb
ep
sph
pl
act
hb

Figure 5

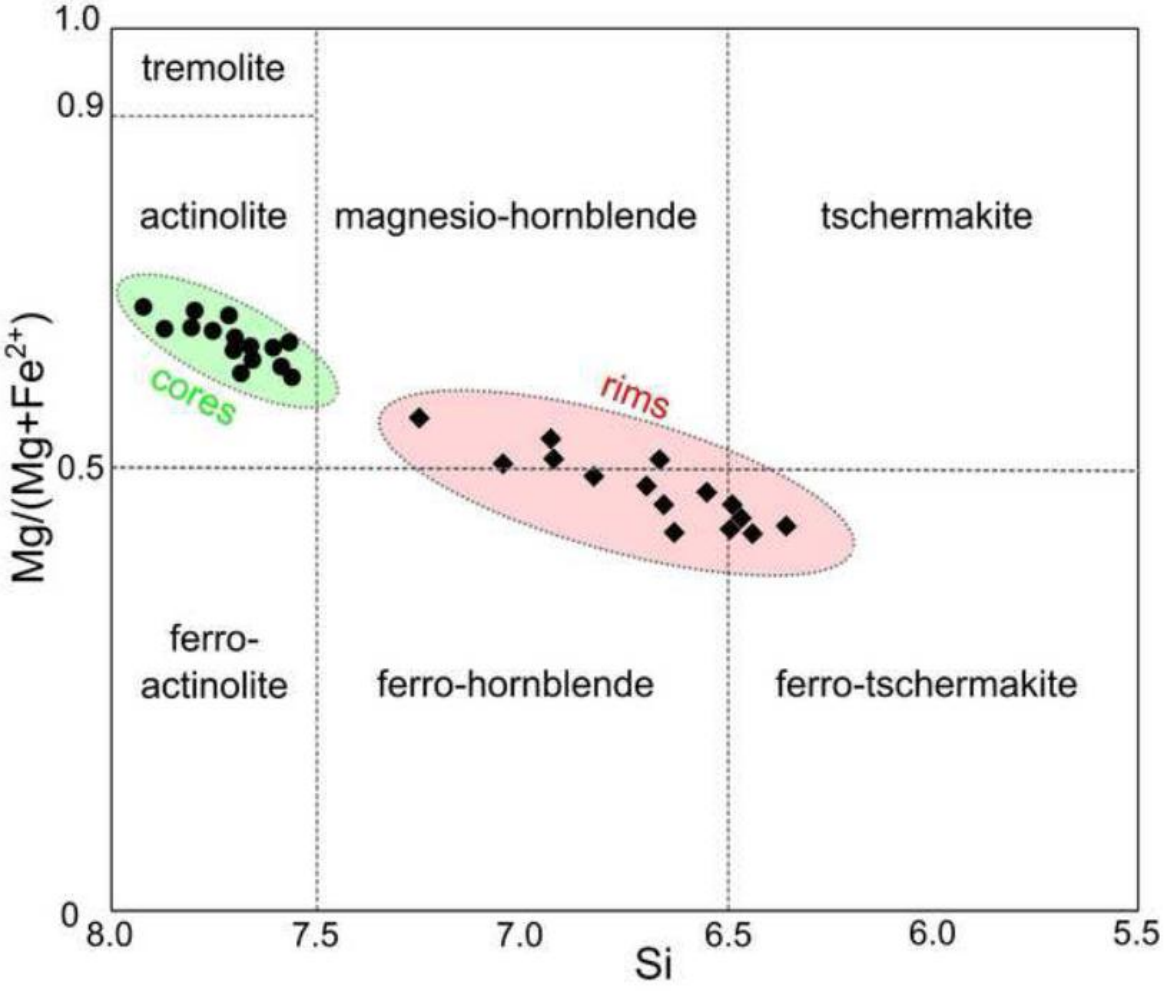

Figure 6

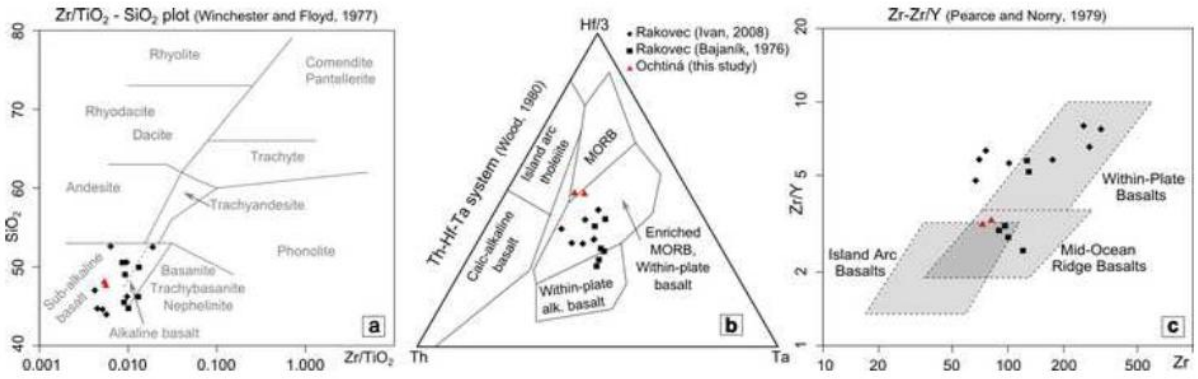

Figure 7

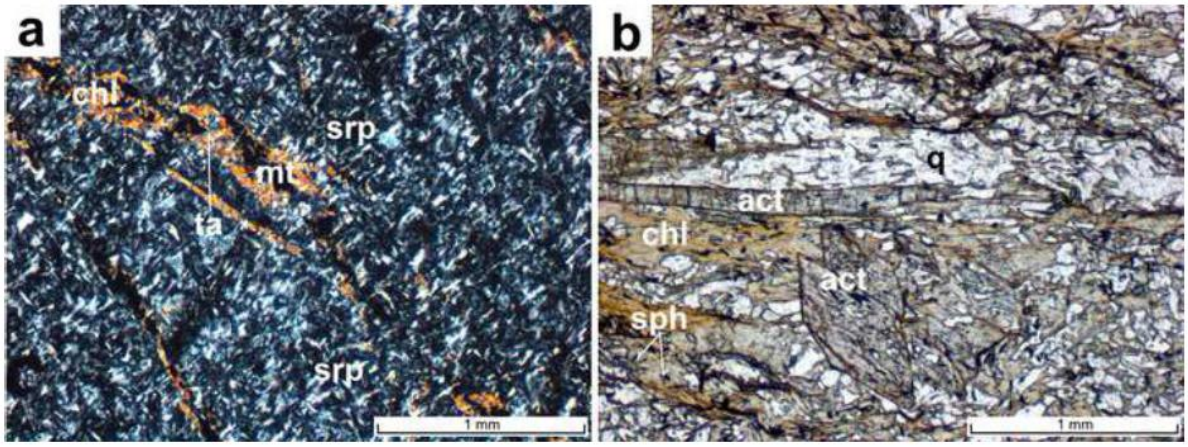

Figure 8

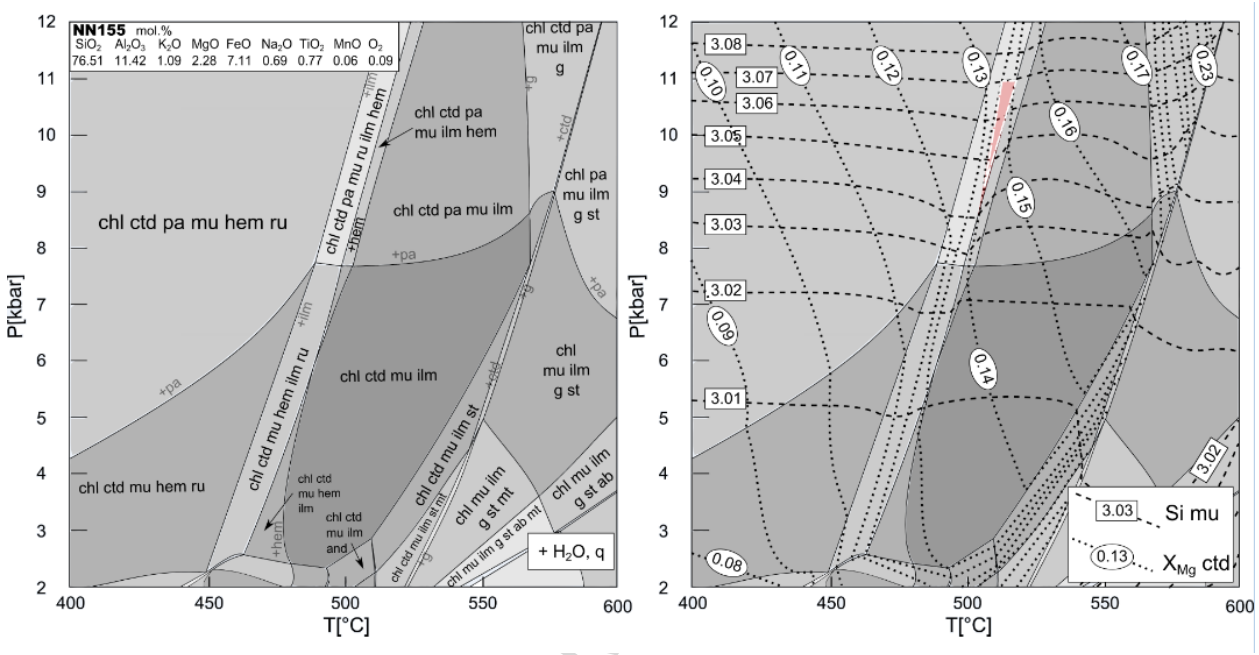

Figure 9

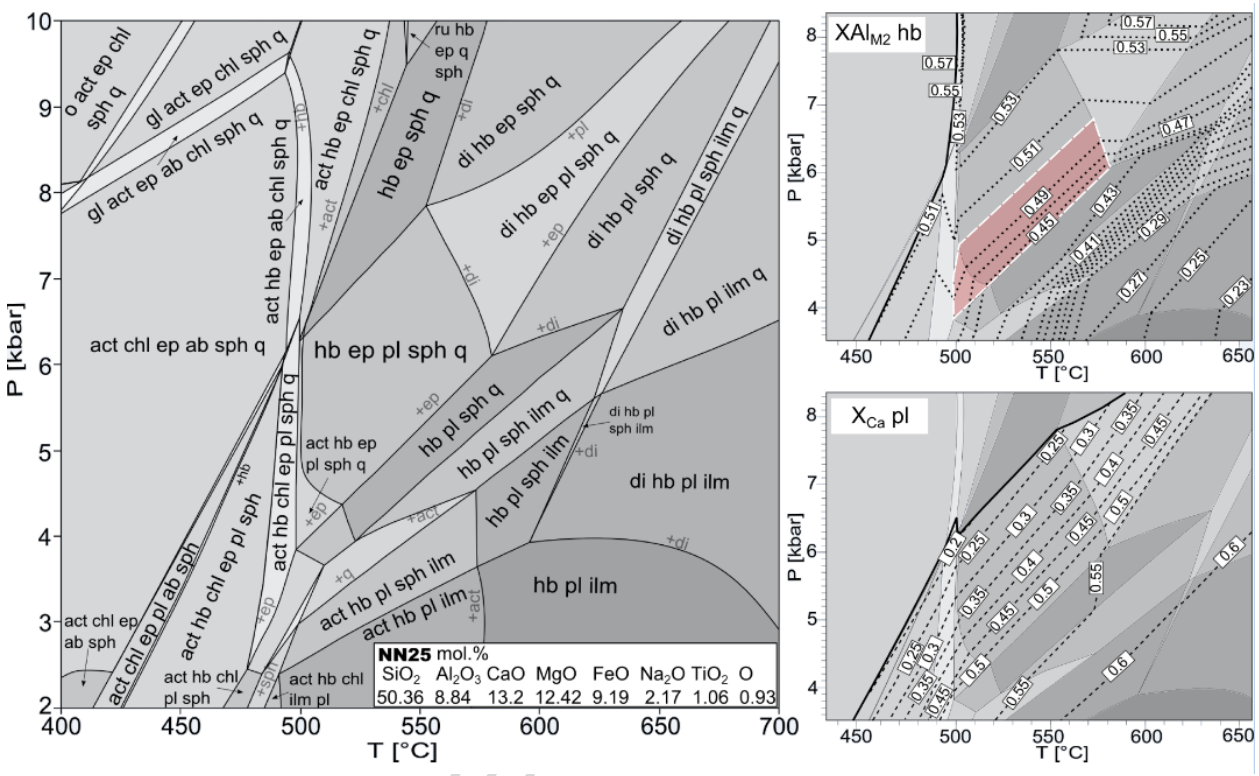

Figure 10

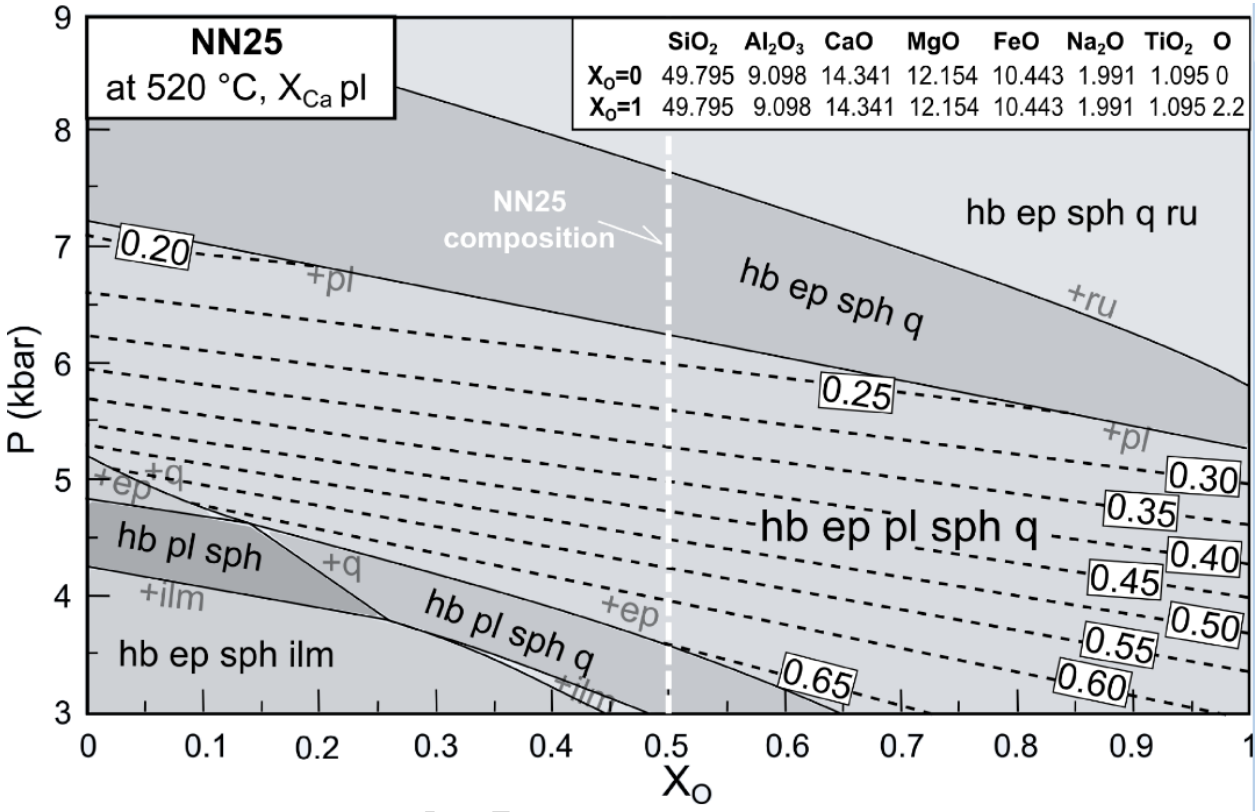

Figure 10

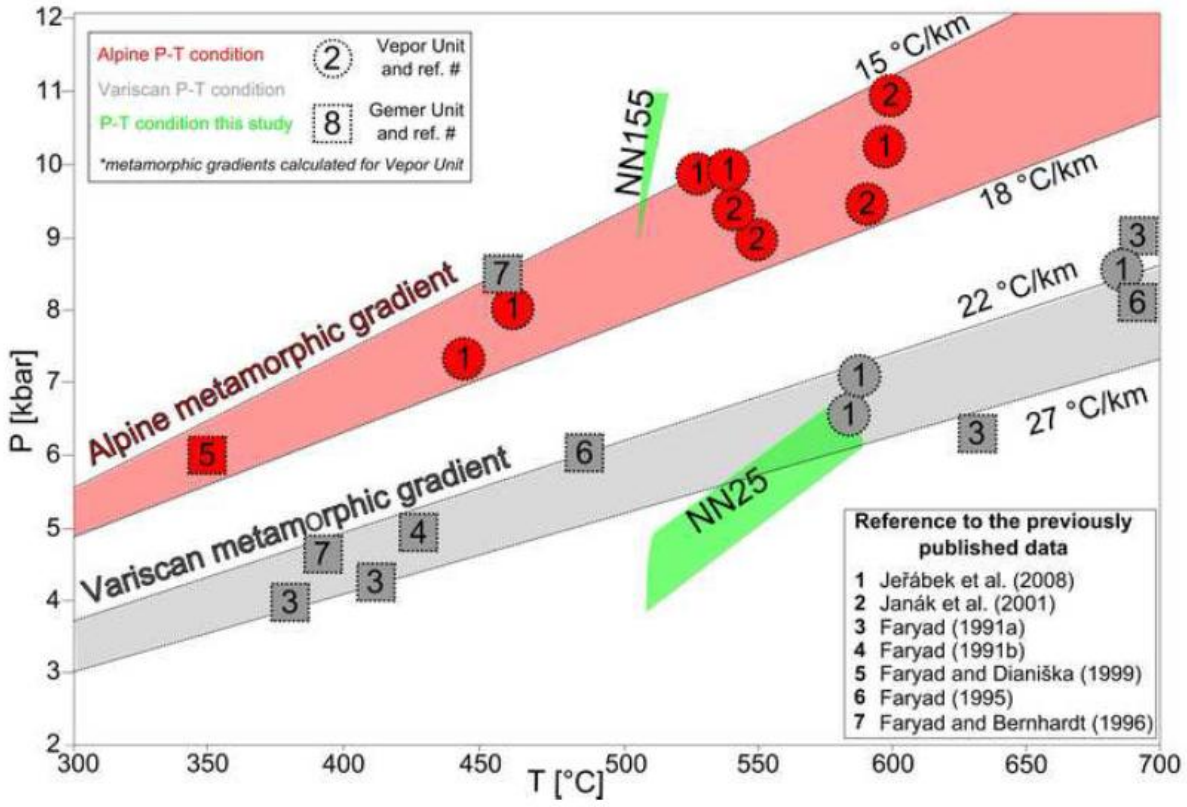

Figure 12

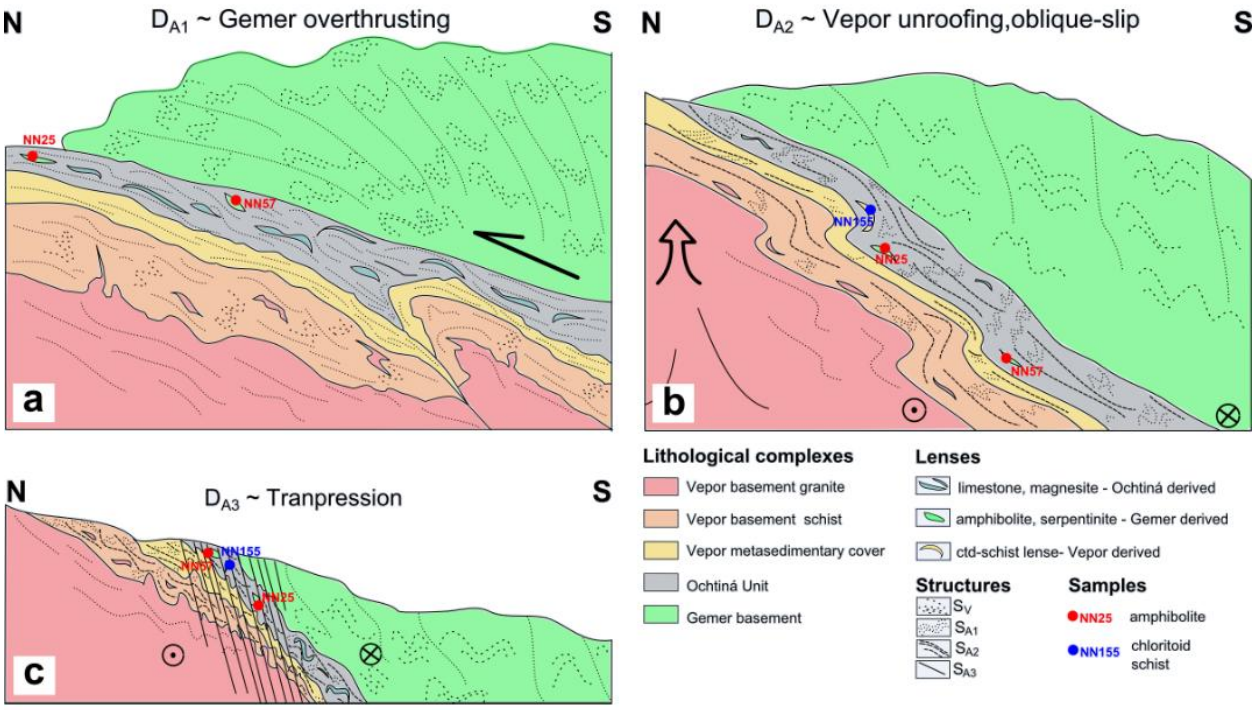

Figure 13